

Article

Effect of Exhaust Gas Recirculation on Combustion Characteristics of Ultra-Low-Sulfur Diesel in Conventional and PPCI Regimes for a High-Compression-Ratio Engine

Charu Vikram Srivatsa, Shah Saud Alam, Bailey Spickler and Christopher Depcik * 

Department of Mechanical Engineering, University of Kansas, 3138 Learned Hall, 1530 W. 15th Street, Lawrence, KS 66045-4709, USA; srivatsacharuvikram@gmail.com (C.V.S.); dr.shah.saud.alam@gmail.com (S.S.A.); spickler.bailey@gmail.com (B.S.)

* Correspondence: depcik@ku.edu; Tel.: +1-785-864-4151

Abstract: Low temperature combustion (LTC) mitigates the nitrogen oxide (NO_x) and particulate matter (PM) trade-off in conventional compression ignition engines. Significant research on LTC using partially premixed charge compression ignition (PPCI) has typically reduced the compression ratio of the engine to control combustion phasing and lower peak temperatures. This study investigates LTC using PPCI with a high-compression-ratio (=21.2) engine by varying fuel injection timing (FIT) from 12.5° to 30.0° before top dead center (BTDC) while modulating EGR (0%, 7%, 14%, and 25%). Advancing FIT led to a gradual rise in the equivalence ratio of the mixture, in-cylinder pressure, temperature, and rate of heat release due to energy losses associated with ignition occurring before the end of the compression stroke. PPCI was successfully achieved with minimal performance impact using a combination of FIT advancements in the presence of high rates of EGR. Specifically, fuel injected at 25.0° BTDC and 25% EGR reduced PM emissions by 59% and total hydrocarbons by 25% compared with conventional FIT (12.5°) without EGR. Moreover, carbon monoxide and NO_x emissions were comparable across set points. As a result, PPCI using high compression ratios is possible and can lead to greater thermal efficiencies while reducing emissions.

Keywords: partially premixed compression ignition; ultra-low-sulfur diesel; exhaust gas recirculation; fuel injection; low temperature combustion; negative temperature coefficient



Citation: Srivatsa, C.V.; Alam, S.S.; Spickler, B.; Depcik, C. Effect of Exhaust Gas Recirculation on Combustion Characteristics of Ultra-Low-Sulfur Diesel in Conventional and PPCI Regimes for a High-Compression-Ratio Engine.

Energies **2024**, *17*, 3950. <https://doi.org/10.3390/en17163950>

Academic Editor: Bo Yang

Received: 25 June 2024

Revised: 26 July 2024

Accepted: 7 August 2024

Published: 9 August 2024



Copyright: © 2024 by the authors. Licensee MDPI, Basel, Switzerland. This article is an open access article distributed under the terms and conditions of the Creative Commons Attribution (CC BY) license (<https://creativecommons.org/licenses/by/4.0/>).

1. Introduction

Diesel-fueled compression ignition (CI) engines deliver more power and have better brake thermal efficiency (BTE) compared with spark ignition (SI) engines, but their high oxides of nitrogen (NO_x) and particulate matter (PM), or soot, are concerning from the standpoint of environmental pollution and global warming [1]. While aftertreatment systems are used with CI engines for emission abatement, these systems are relatively expensive, and their use often lowers fuel efficiency due to the need for treatment after injections to maintain adequate temperature for the optimal conversion of harmful species to less harmful products [2]. Therefore, CI engine technology is undergoing continuous advancement to achieve better fuel efficiency and lower harmful emissions simultaneously [3]; however, understanding combustion in CI engines and the mechanism of NO_x and PM formation becomes important.

CI engine performance and exhaust emissions are influenced by operator behavior and engine runtime parameters such as fuel injection pressure and timing, speed, and load [4]. At the granular level, combustion performance depends on air–fuel mixture quality and its spatial distribution in the combustion chamber. Here, the air–fuel mixture quality is a function of the fuel injection timing (FIT), fuel injection pressure, and compression ratio (CR) of the engine [5,6], whereas its spatial distribution depends on the piston bowl and combustion chamber geometry [7,8]. These parameters govern the formation of a

homogeneous or heterogeneous air–fuel mixture prior to the start of combustion (SOC) and significantly influence combustion characteristics. For example, a uniformly distributed homogeneous air–fuel mixture undergoes combustion that is kinetically controlled by the rate of the reaction with in-cylinder pressure, temperature, type of fuel, and equivalence ratio being the controlling parameters [9].

Once the required autoignition temperature is achieved, the mixture ignites instantaneously without significant temperature and heat flux gradients, resulting in higher flame temperatures, and with the excess availability of oxygen (O_2), a relatively higher combustion efficiency [10]. This phenomenon is alternatively known as pre-mixed combustion. This combination of higher temperatures and excess oxygen creates ideal conditions for NO_x kinetics to dominate at prime crank angles where nitrogen (inducted into the chamber with air) combines with oxygen to form nitric oxide (NO), nitrogen dioxide (NO_2), and nitrous oxide (N_2O) (a potent greenhouse gas) [11,12]. NO_x (a combination of NO and NO_2) is usually formed around the boundary of the fuel spray as depicted in Figure 1.

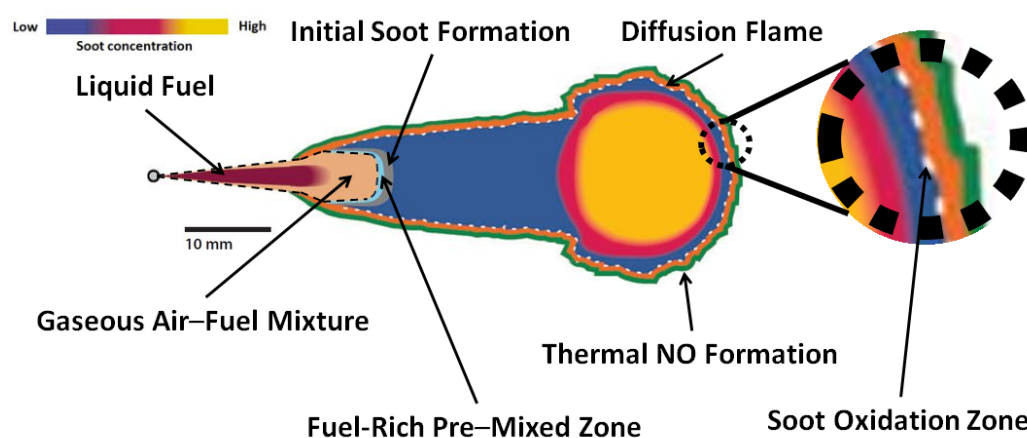


Figure 1. NO_x , PM, and CO_2 chemistry around a fuel spray inside a CI engine. Adapted from [13].

Poor air–fuel mixture quality or spatial distribution leads to a heterogeneous air–fuel mixture, forming fuel pockets in the combustion chamber that auto-ignite at dissimilar times depending on the local equivalence ratio and energy available. In this scenario, the differences in temperature between local conditions and the global chamber are comparatively greater due to the gradients in temperature and heat flux. Hence, heterogeneous air–fuel combustion is often slower because the energy transport becomes a function of the diffusion rate of the gas in the chamber [9]. Alternatively, this phenomenon is called mixing-controlled combustion or, simply, diffusion burn. Slower combustion kinetics are considered a major cause of relatively higher PM emissions, usually in fuel-rich zones like the center of the spray in Figure 1 [13,14].

CI engines often operate nonlinearly under both pre-mixed and diffusion combustion modes; hence, the simultaneous control of both NO_x and PM becomes challenging because the mitigation of one species (say NO_x) results in the growth of the other species (PM) and vice versa. Therefore, research on this NO_x –PM trade-off for the simultaneous abatement of both species has gained traction over the last couple of decades. The available literature shows that low temperature combustion (LTC) and exhaust gas recirculation (EGR) are promising prospects [15,16]. Specifically, LTC was theorized and advanced to decrease both NO_x and PM without compromising engine brake thermal efficiency [17,18]. Under LTC, a pre-mixed air–fuel mixture combusts under lean conditions, resulting in lower heat transfer losses and a shortened combustion duration, thus improving fuel efficiency and lowering emissions, respectively [19].

LTC is categorized into homogeneous charge compression ignition (HCCI), partially pre-mixed charge compression ignition (PPCI, PCCI, or PPCCI), and reactivity-controlled compression ignition (RCCI) combustion modes, which have their respective advantages and disadvantages over conventional diesel combustion (CDC) [20]. Generally, HCCI mode reduces NO_x emissions while achieving high engine BTE; however, the control of combustion phasing is difficult and limited by the load-speed range due to the significant pressure rise at high engine loads and potential misfiring at low engine loads [21–23]. In contrast, RCCI employs the injection of a low-ignition-quality gaseous fuel through the intake port (port fuel injection, or PFI) to enhance the combustion performance of a direct injected (DI) high-ignition-quality liquid fuel while simultaneously lowering exhaust emissions. However, RCCI is difficult to implement in the real world because it requires two separate fuel tanks on board, which increases cost and system complexity [24–28]. In contrast, the PPCI LTC mode is shown in the available literature to operate in between the fully pre-mixed HCCI and fully stratified CDC modes, thus exhibiting the advantages of both [29–32].

The PPCI mode adopts multiple injection strategies, like single or double injection and varied injection timing, and can be merged with exhaust gas recirculation (EGR), as well as combustion chamber modification strategies to offer superior combustion control compared with HCCI, even at higher loads [33–35]. Single- and double-injection strategies combined with PPCI have shown that single-injection events promote pre-mixed combustion (more NO_x), whereas double injection promotes mixing-controlled combustion (more PM) [36–38]. The implementation of PPCI alone faces two major challenges: (a) the chemical kinetics are sensitive to in-cylinder pressure, temperature, and charge composition, which leads to the ignition timing becoming a function of the chemical kinetics, and (b) the fast heat release from spontaneous compression ignition confines the operating range to lower loads [3,39]. A prior effort by the author involved the variation of fuel injection timing (FIT) in a high-compression-ratio CI engine operating under PPCI mode [40]. The varying FIT increased the ignition delay (ID) period and promoted air–fuel mixture homogeneity. This study showed that the ID period remained relatively constant for most cases considered. The high CR of the engine pushed the SOC before the completion of the compression stroke. Moreover, the operation of the engine was restricted to low load conditions to prevent high in-cylinder pressure rates from combustion before top dead center (BTDC), thus ensuring engine safety. Therefore, the extension of ID and the expansion of the operating load conditions become important.

EGR (shown in Figure 2) is often used to do this while also simultaneously reducing NO_x emissions. Since NO_x is usually formed at prime crank angles under high temperature and oxygen-rich conditions, the introduction of EGR into the chamber offsets oxygen and delays NO_x formation [17,41]. Moreover, exhaust gases have heavier molecules, such as carbon dioxide (CO_2) and carbon monoxide (CO), which dilute the charge and remain inert to the combustion reaction, thus lowering in-cylinder temperatures. By decreasing both the in-cylinder oxygen concentration and the combustion temperature, it is possible to reduce NO_x emissions [42–50]. Furthermore, the combustion regime can shift to LTC at high rates of EGR due to the dominance of low-temperature heat release chemical kinetics. This is an important distinction between LTC and conventional combustion, where chemical kinetics predominantly lead to a high-temperature heat release [45,51,52]. Utilizing hot EGR gases also elevates the combustion chamber temperature before SOC, which aids in fuel atomization by evaporating the injected fuel. EGR is the most common strategy to operate in the LTC regime with a stable engine operation [53]. However, employing EGR reduces combustion efficiency and increases brake-specific fuel consumption (BSFC) [42,47,49,54,55]. In addition, increasing the EGR rate reduces the combustion pressure, temperature, and rate of heat release (ROHR) [46,48,56]. As a result, CO, total hydrocarbons (THCs), and PM emissions are generally higher when employing EGR [41–49,52,56–58].

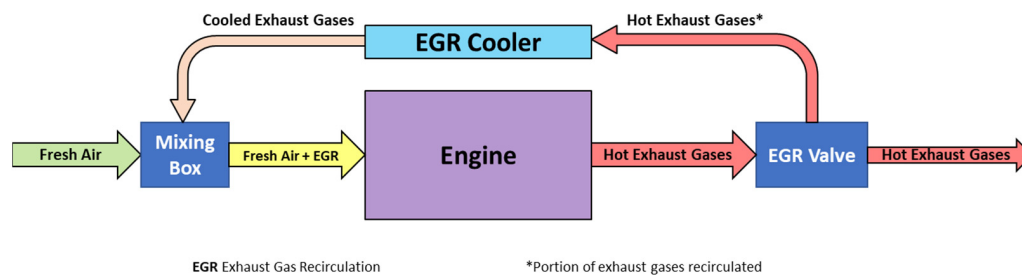


Figure 2. Simple schematic of exhaust gas recirculation (EGR).

The literature illustrates that varying the FIT in the presence of EGR can help in reducing the NO_x -PM trade-off. LTC can be conducted with the PPCI strategy by obtaining instantaneous autoignition of a (largely) homogeneous air–fuel mixture by extending the ID period by modulating the level of EGR and FIT. This approach is applicable for both biodiesel and ULSD utilized in a CI engine [59]. Other techniques, such as employing fuel additives [60,61], water injection [62], and emulsions [61], can also assist in achieving LTC. However, these might not be possible due to restrictions in their practical implementation. Reviewing the literature finds that a significant missing part is the investigation of varying the FIT and EGR to attain LTC in a high-compression-ratio engine. Therefore, experiments using a CI engine with a high compression rate of 21.2 were performed, aiming to achieve PPCI through FIT modulation and EGR strategies. PPCI was successfully achieved using an advanced fuel injection timing (25.0° BTDC) and a relatively high rate of EGR (25%). Both PM and THCs were reduced compared with conventional combustion with comparable CO and NO_x emissions and a minimal impact on performance.

2. Materials and Methods

The engine utilized for testing was a single-cylinder naturally aspirated CI engine. The specifications of the test engine (Yanmar L100V, Yanmar America, Adairsville, GA, USA) and a schematic of the test bed are in Appendix A Table A1 and Figure A1, respectively. A stand-alone EGR system capable of dynamically controlling the EGR rate and temperature was employed [63]. The sensor-measured data were recorded using an in-house built LabVIEW 2017 program in conjunction with National Instruments compact reconfigurable input–output (model #cRIO-9014, Emerson, Austin, TX, USA). This program works as an automated data acquisition software controlled through a laptop computer. The installation of the in-cylinder pressure transducer, the electronic fuel injection system, and the engine data acquisition and control interface were completed by a previous student [64]. In addition, the various sensors and measurement peripherals were set up prior [65]. Details including part numbers and sensitivity information (when applicable) of the dynamometer, fuel and air measurement systems, emission analyzer, and various sensors used are described in the dissertation of the first author [66].

The conventional FIT of the engine is 12.5° and 12.0° BTDC when fueled with ULSD and biodiesel, respectively, at low and medium load conditions. Before testing, the FTIR system was calibrated, and the dynamometer was calibrated through an InterLoc dyno controller. Prior to collecting data, the engine was warmed up until the engine oil temperature and exhaust temperature stabilized (i.e., steady state) with a deviation margin of no more than 2% in $^\circ\text{C}$. The same temperature stabilization criteria were used when FIT/EGR/torque was changed throughout the course of the test before collecting data. The data from all peripheral systems and sensors were collected at 1 Hz, and the in-cylinder pressure was recorded at a crank angle resolution of 0.2° CA. All performance data were collected for 2 min at 1 Hz, and the result presented was the average. Similarly, the emissions from the analyzer were recorded at 1 Hz, and the data presented were the average over a sampling period of 5 min. Additionally, two measurements of the particulate matter, each sampled for 60 s through the smoke meter, were collected and averaged.

Table 1 presents the physical properties of ULSD utilized in this study. Engine operating load conditions were set to be consistent with earlier works to ensure a normalized comparison of results [40]. In this prior effort, FIT was advanced from the conventional 12.5° BTDC to 35° BTDC in steps of 2.5°. Based on the data collected on the same engine, the conclusion of this earlier study indicates that a significant deterioration in combustion performance and emissions occurs for FIT earlier than 30° BTDC. Therefore, 12.5° BTDC to 30.0° BTDC was selected as the limits for the FIT sweep in the current study. A few intermittent FIT points were eliminated as the combustion performance and emission results obtained at these intermittent points were similar and did not add any significant information to the trends observed (discussed in [17]). Only one variable (for example, FIT) was varied while keeping the rest of the operating conditions unchanged.

Table 1. ULSD fuel properties [64].

Property	ULSD
Density (kg/m ³)	839.60 ± 0.01
Kinematic Viscosity (cSt)	2.481 ± 0.001
Dynamic Viscosity (cP)	2.083 ± 0.001
Cetane Number (-)	42.3
Energy Content (kJ/kg)	45,494 ± 44
H/C Molar Ratio	1.80 ± 0.04

With respect to EGR, experiments were conducted to estimate the maximum EGR rate achievable at low load conditions. EGR is defined as follows:

$$\text{EGR} = \frac{\text{CO}_2^{\text{In}} - \text{CO}_2^{\text{Amb}}}{\text{CO}_2^{\text{Ex}} - \text{CO}_2^{\text{Amb}}} \times 100, \quad (1)$$

where CO_2^{In} , CO_2^{Amb} , and CO_2^{Ex} are the inlet, ambient, and exhaust carbon dioxide levels, respectively. It was found that 25% EGR was the maximum attainable EGR rate. The 0% to 25% span was split into four approximate quarters, and 0%, 7%, 14%, and 25% EGR rates were selected as the intermediate operating points. This was performed to assist in identifying any potential differences in combustion performance and emission behavior with increasing EGR. Table 2 supplies the FIT, EGR, and engine load settings at which engine performance and emissions data were collected. Since the combustion performance and emission trends of all three load conditions were similar, only the 1.5 N-m load results are discussed. The results of the 0.5 N-m and 1.0 N-m tests are given in Appendix A. The choice of presenting the results using torque ensures consistency with the reporting of earlier efforts. Graphs of the indicated mean effective pressure (IMEP) are also provided in Appendix A.

Table 2. Engine operating load conditions and associated EGR and FIT settings.

Target Engine Loads (N-m)	FIT (° BTDC)	Target EGR Rates (%)
0.5, 1.0, and 1.5	12.0, 15.0, 20.0, 25.0, and 30.0	0.0, 7.0, 14.0, and 25.0

A zero-dimensional heat release model was employed to compute thermodynamic parameters, such as the in-cylinder temperature, ROHR, ID period, and SOC timing [67]. The in-cylinder temperature and ROHR (dQ_{HR}/dt) were calculated using the ideal gas law and the first law of thermodynamics, respectively. The generalized version of the first law is as follows:

$$\frac{dQ_{HR}}{dt} = \frac{dU_{CV}}{dt} - \frac{dQ_{HT}}{dt} + \frac{dW_{CV}}{dt} - \sum_{in} \dot{m}_{in} h_{in} + \sum_{ex} \dot{m}_{ex} h_{ex} \quad (2)$$

This equation includes the change in internal energy (dU_{CV}/dt), heat transfer rate (dQ_{HT}/dt), power (dW_{CV}/dt), and the impact of inlet and exit enthalpy flows while assuming negligible potential and kinetic energies. The ID period and SOC timing were determined using the second derivative of the in-cylinder pressure, which is a well-established method in the literature, as discussed by Mattson et al. [67].

Additional performance parameters calculated include the equivalence ratio, brake-specific fuel consumption, and brake-specific emissions. The equivalence ratio (ϕ) is determined from the mass flow rates of air (\dot{m}_a) and fuel (\dot{m}_f) as compared with the stoichiometric air-to-fuel ratio (AF_s) of 14.6, as follows:

$$\phi = \frac{AF_s}{\dot{m}_a/\dot{m}_f} \quad (3)$$

The brake-specific fuel consumption ($bsfc$) is calculated from the fuel flow rate and brake power (P_b), as follows:

$$bsfc = \frac{\dot{m}_f}{P_b} \quad (4)$$

and the brake-specific emissions (bs_{xx}) are determined from the mass flow rate of emissions (\dot{m}_{xx}) and the brake power, as follows:

$$bs_{xx} = \frac{\dot{m}_{xx}}{P_b} \quad (5)$$

3. Results and Discussion

3.1. Effect of Advancing FIT—Combustion Characteristics

Figure 3 highlights the influence of FIT on the equivalence ratio of ULSD. For the 0% EGR case, advancing the FIT from the maximum brake torque (MBT) timing (12.5° BTDC) led to a gradual increase in the equivalence ratio for all three load conditions. This was due to the early onset of combustion and its associated energy loss, as explained in the following section. EGR rates of 7%, 14%, and 25% showed similar trends of increasing fuel consumption with advancing FIT.

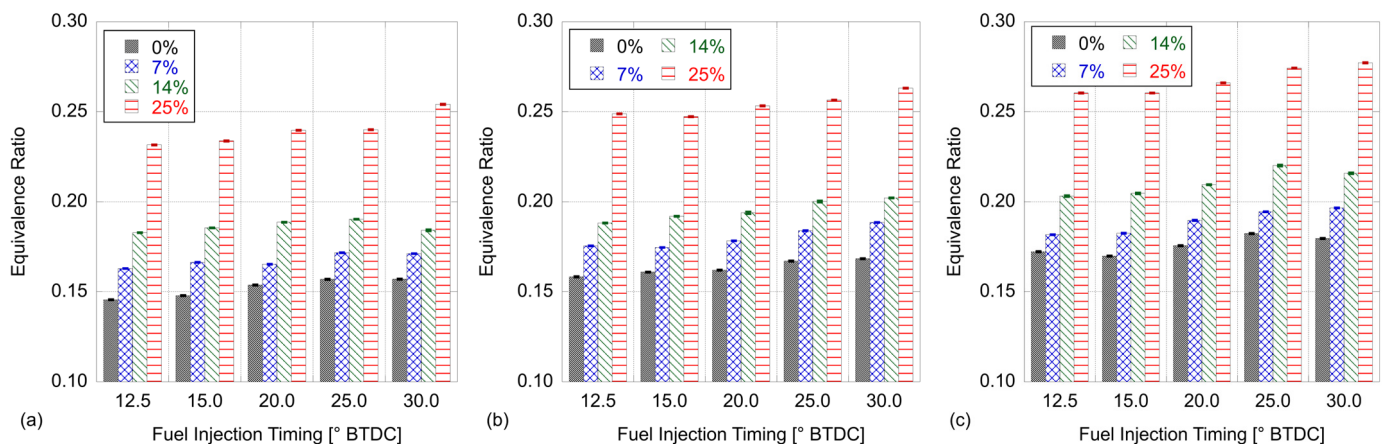


Figure 3. Equivalence ratio vs. FIT at (a) 0.5 N-m, (b) 1.0 N-m, and (c) 1.5 N-m load conditions for ULSD with EGR.

The fuel consumed was highest for the 1.5 N-m (Figure 3c) load condition and least for the 0.5 N-m (Figure 3a) load condition at all EGR and FIT set points considered in Figure 3. As expected, running at higher loads requires more fuel. At each load, it was predicted that BSFC would gradually rise with advancing FIT due to an increase in the level of fuel needed to maintain engine load while heat transfer losses grew. However,

there is no clear trend noticeable in Figure 4a due to difficulties associated with maintaining a constant engine torque during the data acquisition period. As depicted in Figure 4b, the actual engine torque is marginally higher or lower than the required setting (1.5 N-m). Here, the ultra-lean operating conditions cause combustion variability, hence skewing the BSFC trends.

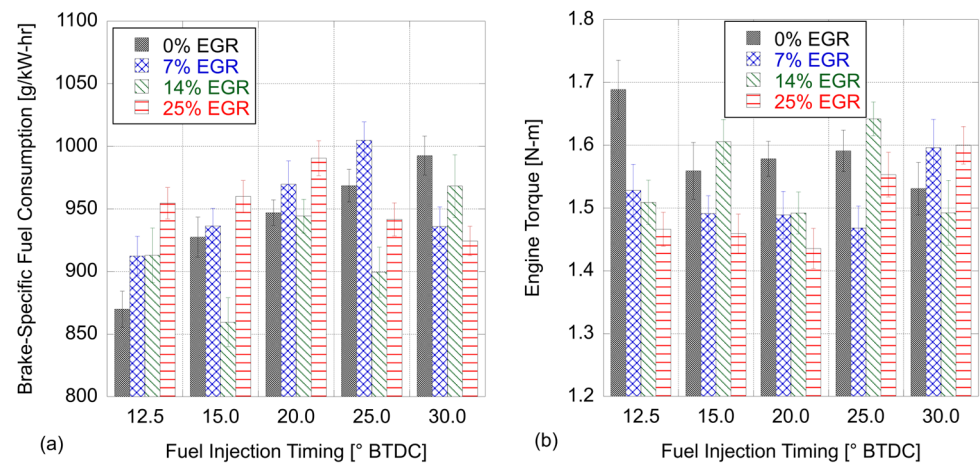


Figure 4. (a) BSFC and (b) engine torque vs. FIT at 1.5 N-m load condition for all EGR rates with ULSD.

With respect to performance parameters, advancing FIT generally resulted in a gradual growth in in-cylinder pressure (Figure 5a), temperature (Figure 5b), and ROHR (Figure 5c) for the 0% EGR rate. In addition, the timing of the peak in-cylinder pressure ($\theta\text{-max}_{\text{Pressure}}$), temperature ($\theta\text{-max}_{\text{Temperature}}$), and ROHR ($\theta\text{-max}_{\text{ROHR}}$) happened earlier during the compression stroke while advancing FIT. The values of peak in-cylinder pressure (Figure 6a), temperature (Figure 6b), and ROHR (Figure 6c) and the corresponding crank angle of maximum pressure ($\theta\text{-max}_{\text{Pressure}}$), temperature ($\theta\text{-max}_{\text{Temperature}}$), and ROHR ($\theta\text{-max}_{\text{ROHR}}$) are provided in Figure 6d, Figure 6e, and Figure 6f, respectively, to assist in understanding these trends. Similar results of advancing $\theta\text{-max}_{\text{Pressure}}$, $\theta\text{-max}_{\text{Temperature}}$, and $\theta\text{-max}_{\text{ROHR}}$ and rising in-cylinder pressure and ROHR with FIT advancement were obtained by other researchers [48,52,54,57,68]. The ignition timing moves earlier into the compression stroke as FIT is advanced. This is illustrated through the divergence of the in-cylinder pressure curve away from the motoring trace.

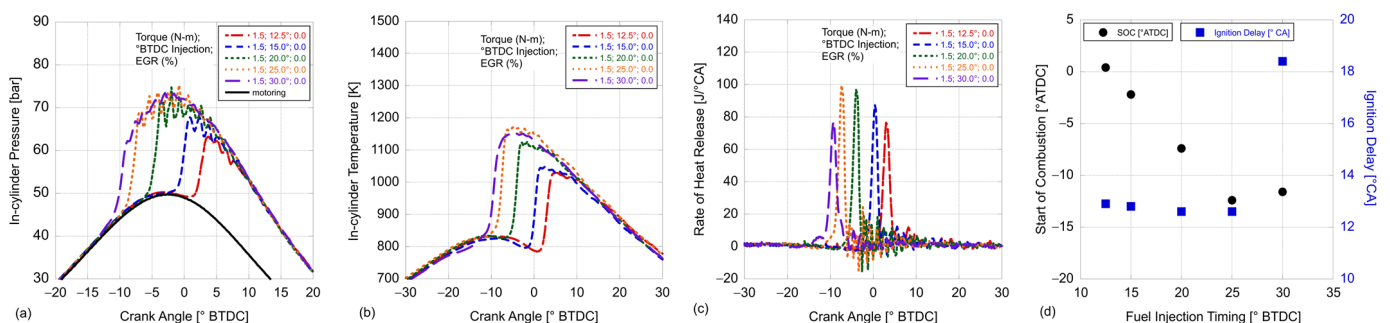


Figure 5. (a) In-cylinder pressure, (b) in-cylinder temperature, (c) ROHR, and (d) ID and SOC vs. FIT at 1.5 N-m load condition for 0% EGR with ULSD.

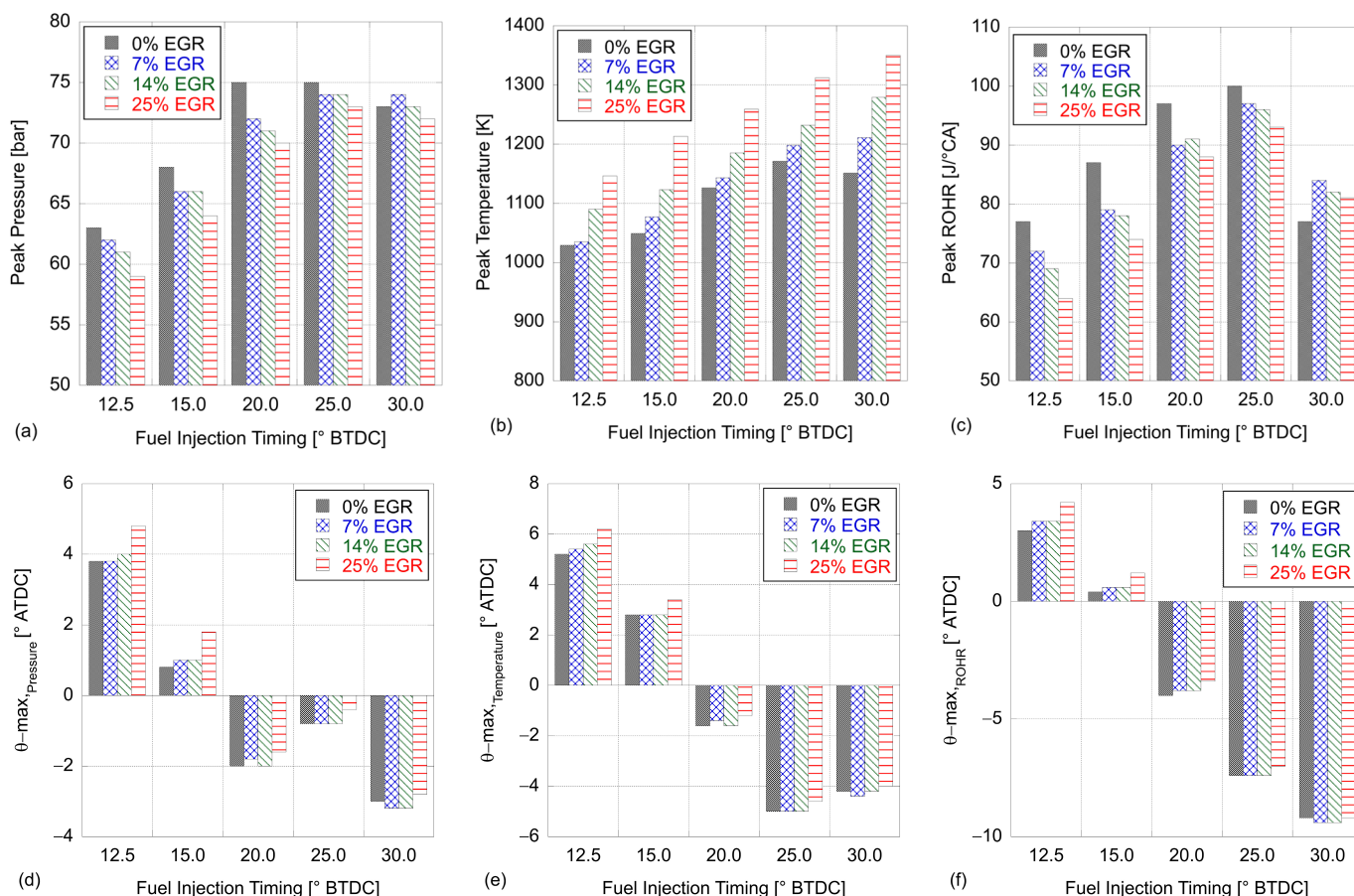


Figure 6. Peak in-cylinder (a) pressure, (b) temperature, (c) ROHR, and corresponding crank angle position of (d) pressure, (e) temperature, and (f) ROHR vs. FIT for 1.5 N-m load condition with ULSD.

The SOC and ignition delay details presented in Figure 5d also reflect this outcome. Since ignition occurs a few degrees before TDC for fuel injected at 15.0° BTDC and earlier, the interaction between the compressing piston and the combustion process results in a double compression effect. Generally, most of the expended energy is recaptured during the expansion stroke. The interaction of the flame with the compressing gases increases its interaction with the wall, resulting in combustion flame quenching. In addition, advancing the SOC timing into the compression stroke gradually increases energy losses through heat transfer. Thus, keeping a constant engine load requires a further fuel addition due to the combination of energy loss through flame quenching and heat transfer losses. This results in the higher equivalence ratio observed in Figure 3 and the corresponding in-cylinder pressure (Figure 6a), temperature (Figure 6b), and ROHR (Figure 6c) growth for FIT events between 12.5° and 25.0° BTDC.

Oscillations in the pressure curve signifying CI knock were seen for most set points. These oscillations were relatively negligible for the 30.0° BTDC event, suggesting a gradual combustion of a comparatively more homogeneous air–fuel mixture (also seen in a prior work [40]). Here, CI knock was analyzed solely on observed oscillations in the in-cylinder pressure curve, and no extensive knock analysis was performed. Moreover, the peak in-cylinder pressure, temperature, and ROHR for the 30.0° BTDC event were marginally lower than those for the 25.0° BTDC event (Figure 6a–c). In addition to greater heat transfer losses, this decline in ROHR seen at 30.0° BTDC could be due to (a) transition in combustion from conventional to LTC or (b) deteriorating combustion efficiency. The emission results and the comparison of ID versus in-cylinder temperature at the corresponding FIT (presented later) will assist in making this conclusion.

Figure 6d highlights a shift in the trend of $\theta\text{-max}_{\text{Pressure}}$. As FIT is advanced between 12.5° and 20.0° BTDC, $\theta\text{-max}_{\text{Pressure}}$ moves into the compression stroke. It shifts towards TDC for fuel injected at 25.0° BTDC. This is due to the negative temperature coefficient (NTC) characteristics of ULSD in CI engines, which will be explained in the following section with the aid of ID versus in-cylinder temperature plots.

The ID marginally reduces as the FIT is advanced between 12.5° and 20.0° BTDC (Figure 5d) for the 0% EGR case. The ID period for the 20.0° and 25.0° BTDC events are comparable. In general, this suggests that the high CR of the engine (21.2) ensures that the in-cylinder pressure and temperature when fuel is injected are sufficiently high for the vaporization and later ignition of the fuel. This is the case even though there is a reduction in in-cylinder temperature when FIT is advanced between 12.5° and 30.0° BTDC (Figure 7a).

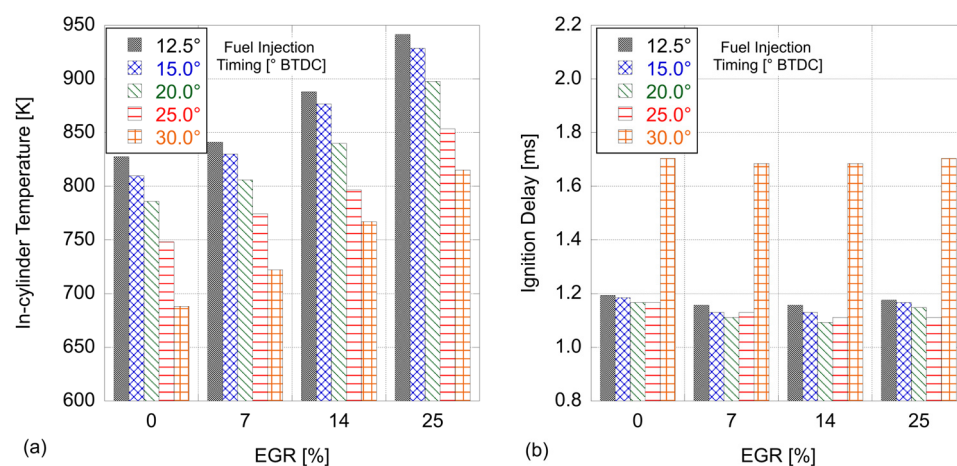


Figure 7. (a) In-cylinder temperature at the corresponding FIT and (b) ID vs. EGR rate at 1.5 N-m with ULSD.

The ID decreases gradually for FIT advancement between 12.5° and 25.0° BTDC, as seen in Figure 7b and Table 3. As explained in an earlier work, this is due to the NTC behavior of ULSD [17,69–72]. Briefly, at high initial temperatures, air–fuel mixtures prefer a channel propagation pathway, resulting in ignition, followed by a high energy release. Alternatively, at lower initial temperatures, ULSD prefers a chain branching pathway for its later ignition. The reactivity of the charge increases during the transition from the channel propagation to the branch propagation pathways or due to the competition in the two available pathways. In other words, a temperature window exists in which the decreasing initial temperature causes an increase in the reactivity of the system. This is called the NTC region. A lower ID period is a well-known characteristic of air–fuel mixtures in the NTC region [69–72]. For instance, the ID periods for the fuel injected at 12.5° and 15.0° are greater than the 20.0° and 25.0° events even though temperatures in the cylinder when fuel is injected are higher for the former events (Figure 7a).

Alternatively, there is a sharp rise in the ID for the injected fuel at 30.0° BTDC. This is also reflected by the SOC trend, which sharply deviates from the (almost) linear pattern for the 30.0° BTDC event (Figure 5d). This shows that the in-cylinder temperature and pressure conditions in the cylinder when fuel is injected switch the kinetics to a pathway that has a comparatively lower reactivity. Additionally, the lower in-cylinder pressure at the corresponding FIT enhances fuel penetration, resulting in possible fuel wall wetting. The fuel that adheres to the combustion chamber walls (also known as wall wetting) does not take part in the main combustion process. This can be further proven through incomplete combustion products (CO and THC emissions), as described in the following section. As a result, it can be assumed that this extended ID provides the necessary time to create an air–fuel mixture with better homogeneity as compared with conventional combustion. It is

imperative to say that the air–fuel mixture for fuel injected at 30.0° BTDC is still stratified, especially, in contrast with the homogeneity of mixtures obtained through PFI systems.

Table 3. Ignition delay period and in-cylinder temperature at the corresponding FIT for all set points considered at 1.5 N-m load condition.

		FIT [° BTDC]				
EGR Rate		12.5	15	20	25	30
0%	ID [ms]	1.194 (Δ)	1.185	1.167	1.167	1.704
7%		1.157	1.130	1.111	1.130	1.685
14%		1.157	1.130	1.093	1.111	1.685
25%		1.176	1.167	1.148	1.111	1.704 (Δ)
		FIT [° BTDC]				
EGR Rate		12.5	15	20	25	30
0%	In-cylinder temperature at FIT [K]	770.93	767.04	733.98	699.81	651.54
7%		782.21	777.67	742.10	706.93	658.71
14%		784.79	778.74	743.76	710.64	660.12
25%		788.55	781.52	746.39	710.49	661.18

Subsequently, the in-cylinder pressure, temperature, ROHR, SOC, and ID trends for 7% EGR (Figure 8), 14% EGR (Figure 9), and 25% EGR (Figure 10) are comparable with the no-EGR case. As depicted in Figures 8a, 9a and 10a, analogous to the 0% EGR case, as FIT is advanced, the magnitude of peak pressure gradually rises for FIT between 12.5° and 25.0° BTDC. In addition, the combustion pressure declines marginally for 30.0° FIT compared with the 25.0° BTDC event. Like the 0% EGR case, $\theta\text{-max}_{\text{Pressure}}$ (Figure 6d) moves into the compression stroke between 12.5° and 20.0° BTDC for the 7%, 14%, and 25% EGR rates. However, $\theta\text{-max}_{\text{Pressure}}$ shifts towards TDC for the 25.0° BTDC for all three EGR cases. The oscillations in the pressure curve are negligible for the 30.0° BTDC events.

Like the combustion pressure, the combustion temperature and ROHR trends for the 7% (Figure 8b,c), 14% (Figure 9b,c), and 25% (Figure 10b,c) EGR cases are comparable with the 0% EGR case. Combustion temperature (Figure 6b) gradually increased as FIT was advanced due to the excess fuel injected. This excess fuel is needed to compensate for the energy loss through heat transfer, double compression effect, and flame quenching to keep a constant operating load. The combustion temperature and ROHR marginally declined for fuel injected at 30.0° compared with the 25.0° BTDC event.

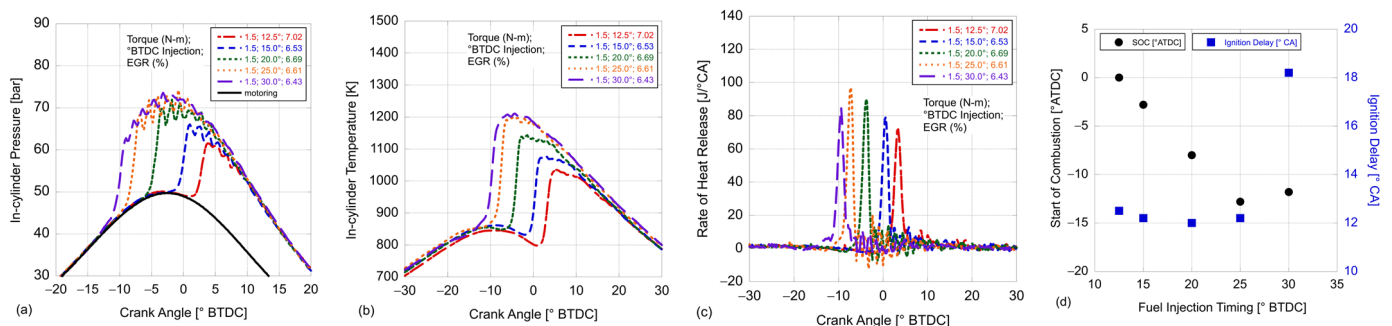


Figure 8. (a) In-cylinder pressure, (b) in-cylinder temperature, (c) ROHR, and (d) ID and SOC vs. FIT at 1.5 N-m load condition for 7% EGR with ULSD.

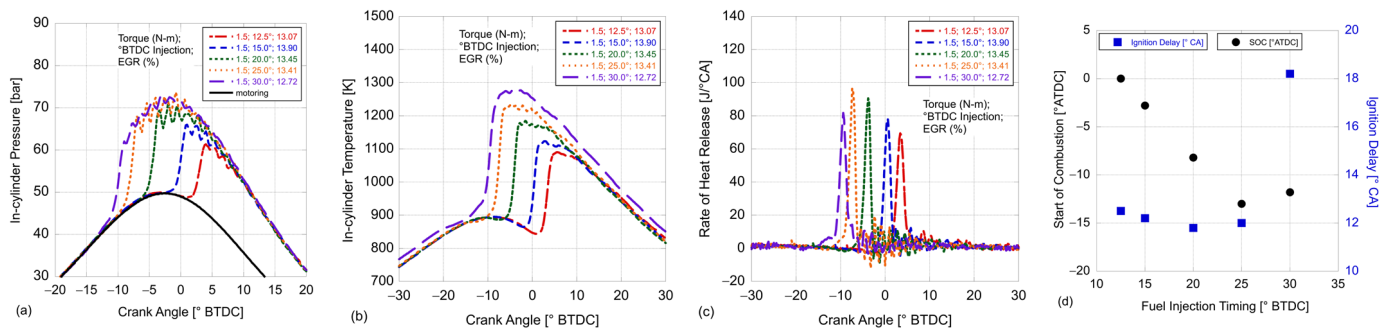


Figure 9. (a) In-cylinder pressure, (b) in-cylinder temperature, (c) ROHR, and (d) ID and SOC vs. FIT at 1.5 N-m load condition for 14% EGR with ULSD.

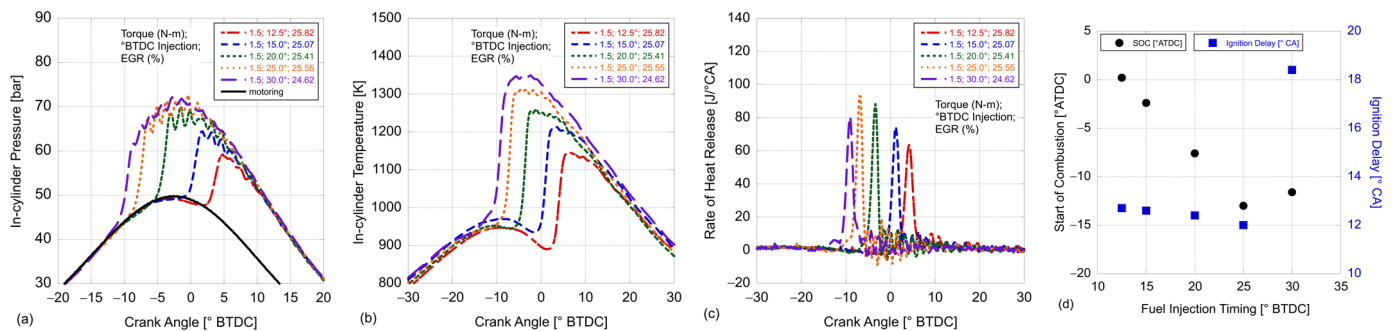


Figure 10. (a) In-cylinder pressure, (b) in-cylinder temperature, (c) ROHR, and (d) ID and SOC vs. FIT at 1.5 N-m load condition for 25% EGR with ULSD.

The ID and SOC trends for the 0%, 7% (Figure 8d), and 14% EGR (Figure 9d) cases were comparable. Recalling the temperatures in the cylinder when fuel was injected, advancing FIT gradually reduced the temperature for the 7%, 14%, and 25% EGR rates. The ID decreased with FIT advancement between 12.5° and 20.0° BTDC. Therefore, a noticeable temperature window existed, where the decreasing temperature led to a marginal decrease in the ID period, as seen in Figure 7b. The lowest ID for the 0%, 7%, and 14% EGR cases was observed for fuel injected at 20.0° BTDC.

The lowest ID for the 25% EGR case occurred for FIT at 25.0° BTDC. This marginal difference in the ID shift seen could be due to cyclic variations or caused by a change in the kinetic behavior in the NTC region due to the presence of excess CO₂ and/or due to the lack of O₂. Unfortunately, there are no kinetic studies reported in the literature that support or reject this theory. Like the 0% EGR case, the ID period stays comparable at 25.0° BTDC while increasing significantly at 30.0° BTDC for the 7%, 14%, and 25% EGR rates. As discussed earlier, this is caused by an assumed increase in cylinder wall wetting due to fuel penetration, which slows down the atomization and ignition process.

3.2. Effect of Increasing EGR—Combustion Characteristics

Increasing the rate of EGR from 0% to 7% led to an approximately 10% rise in equivalence ratio, as shown in Figure 3. This was true for all FIT and load conditions. Similarly, a further 10% (approximate) rise in the equivalence ratio was seen as EGR was raised from 7% to 14%. For the 25% EGR set point, there was a sharp increase in the equivalence ratio seen (between 25% and 28%) compared with the 14% EGR case. In summary, the equivalence ratio for the 25% EGR case was about 52% to 57% higher than the 0% EGR set point. The highest equivalence ratio recorded is approximately 0.26 for the 1.5 N-m load condition with 25% EGR. Therefore, sufficient O₂ is still available in comparison with the amount of fuel injected. Increasing EGR typically leads to an elevated BSFC due to a growing level of fuel required to meet the engine load [48,51,52,56]. However, the BSFC

data shown in Figure 4a do not show a specific trend. As discussed earlier, the cyclic combustion variations of the engine apparently skew the trend of BSFC (Figure 4b).

The in-cylinder pressure, temperature, and ROHR decrease with an increasing EGR rate (see Figure 5). As the EGR rate increases, the amount of O₂ displaced by CO₂ and H₂O rises. The general trend of declining combustion temperature, pressure, and ROHR is due to the following:

1. The excess CO₂ and H₂O in the intake acts as a diluent (i.e., heat sink) and is mostly inert, hence reducing the charge reactivity in the combustion chamber.
2. The reduction in the availability of O₂ lowers the rate of oxidation of the hydrocarbons, resulting in lower chemical energy released. Additionally, the released energy is absorbed by CO₂ and H₂O since they have a higher heat capacity.
3. Since EGR is relatively hot, the higher temperature when fuel is injected assists with fuel evaporation and results in a subsequent earlier SOC. Increasing EGR lowers the ID period, which results in less constant volume-like combustion.
4. Somewhat counterbalancing these effects is the greater equivalence ratio, which results in a higher adiabatic flame temperature.

As expected, the size of the peak pressure marginally declined for all FIT set points (Figure 6a) with increasing EGR. The maximum decline in pressure between the 0% and 25% EGR rates was about 6.4% for fuel injected at 12.5° and 20.0° BTDC (Table 4). The corresponding minimum decline was about 2%, as seen for the 30.0° BTDC event. Analogous to the pressure, temperature in the cylinder gradually declines with an increasing EGR rate for all FIT points (Figure 6b). A maximum in-cylinder temperature decline of 4.2% was seen at 12.5°, and a minimum of 2.6% was seen at 30.0° BTDC. Overall, the decrease in pressure and temperature are relatively low. Finally, the ROHR gradually decreases with increasing EGR for all FITs considered (Figure 6c). The size of decline between the 0% and 25% EGR rates was relatively high for fuel injected at 12.5° (16.9%) and 15.0° (15.1%). Subsequently, for the 20.0° and 25.0° events, the corresponding decline was only about 8.8% and 6.6%, respectively. For the fuel injected at 30.0° BTDC, increasing EGR from 0% to 25% resulted in a 7.4% decline in the ROHR.

Table 4. Maximum decrease in performance parameters for increasing EGR from 0% to 25% at 1.5 N-m load condition with ULSD.

FIT [° BTDC]	Maximum Decrease between 0% and 25% EGR		
	Pressure [%]	Temperature [%]	ROHR [%]
12.5	6.4	4.2	16.9
15.0	5.0	3.2	15.1
20.0	6.4	3.6	8.8
25.0	3.5	3.1	6.6
30.0	1.8	2.6	7.4

With respect to ID, the reduction in the reactivity of the system is expected to extend the ID period with an increasing EGR. On close observation of the ID data presented in Table 5, the ID period marginally drops (about 3–4%) when the EGR rate is increased from 0% to 7% for all FIT set points. When raising the EGR rate from 7% to 14%, the ID stays relatively unchanged for FITs of 12.5° and 15.0° BTDC. Subsequently, the ID decreases by about 1.6% for fuel injected at 20.0° and 25.0°. By introducing hot EGR gases, the cylinder temperature at the corresponding FIT slightly rises with an increasing EGR rate for all FIT set points (Figure 7). This suggests that the rise in the initial temperature of the charge due to the hot EGR gasses contributes to the reduction in the ID period [10]. In addition, the amount of fuel injected rises gradually with increasing EGR, resulting in higher adiabatic flame temperatures, which also reduces the ID.

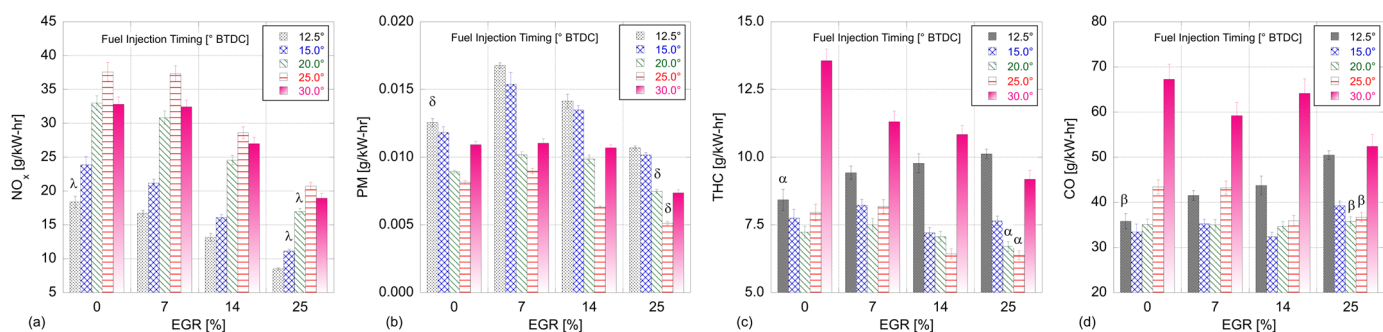
Table 5. Ignition delay period for all set points considered at 1.5 N-m load condition for ULSD.

EGR Rate	FIT [° BTDC]	ID [ms]				
		12.5	15.0	20.0	25.0	30.0
0%		1.194 (Δ)	1.185	1.167	1.167	1.704
7%		1.157	1.130	1.111	1.130	1.685
14%		1.157	1.130	1.093	1.111	1.685
25%		1.176	1.167	1.148	1.111	1.704 (Δ)

For the final bump in the EGR rate from 14% to 25%, the ID marginally increases for all FIT set points, except for fuel injected at 25.0° BTDC, for which the ID stays constant. This shows that the charge reactivity begins to decline due to the increase in diluents, such as CO₂ and H₂O. Comparing the no-EGR case and the 25% EGR setting, the ID is marginally lower for the 25% EGR case for FITs between 12.5° to 25.0° BTDC. Finally, the ID is still relatively constant for fuel injected at 30.0° BTDC for all EGR rates with a maximum difference of 1.1%. This suggests that the lower cylinder pressure at the corresponding FIT has a dominating effect on the ID compared with the EGR rate. Here, wall wetting at 30.0° BTDC due to fuel penetration could contribute to this extension in the ID period, as indicated in Table 5.

3.3. Effect of Advancing FIT—Emissions

Brake-specific NO_x, PM, CO, and THC emissions for the 1.5 N-m load condition for all FIT and EGR settings are presented in Figure 11. The uncertainty analysis of the brake-specific emission data was performed and found that the uncertainty was less than $\pm 4.7\%$ for all emission species presented in the 1.5 N-m load condition. In addition, the uncertainty was less than $\pm 5.4\%$ for all emission species for the 0.5 N-m and 1.0 N-m load conditions. To aid in the clean presentation of the data, the uncertainty results are not incorporated into the graphs.

**Figure 11.** (a) NO_x, (b) PM, (c) CO, and (d) THC emissions for varying EGR rates at 1.5 N-m load condition with ULSD.

NO_x emissions gradually increase between 12.5° and 25.0° BTDC, as depicted in Figure 11a. As discussed earlier, the in-cylinder temperature for these injection events rises with FIT advancement along with more time for NO_x kinetics, hence leading to elevated NO_x generation. Since the maximum equivalence ratio is only about 0.26 for the 1.5 N-m load condition, abundant O₂ is available for NO_x production via the thermal NO_x mechanism. However, there is a marginal decline in the NO_x emissions for the 30.0° BTDC event due to the lower in-cylinder temperature obtained (Figure 6). This can also be correlated with the rise in the products of incomplete combustion, CO (Figure 11c) and THC (Figure 11d), for the 30.0° BTDC event. Thus, this drop in NO_x emissions is also due to declining combustion efficiency.

PM emissions declined for the FIT advancement between 12.5° and 25.0° BTDC, as shown in Figure 11b. The rising combustion temperature and the lean operating conditions led to this decrease in PM seen even though the ID decreased, resulting in a slightly more heterogeneous combustion process. Additionally, PM emissions marginally increased for the 30.0° case as compared with the 25.0° event. The NO_x and PM emissions for all EGR rates had the opposite trend as FIT was advanced, hence following the traditional NO_x-PM trade-off. Therefore, advancing FIT alone has no success in alleviating the NO_x-PM trade-off for ULSD.

As the injection timing is advanced between 12.5° and 20.0°/25.0° BTDC, THC emissions gradually decrease. As shown earlier, the temperature in the cylinder and ROHR gradually increases for these set points, aiding in the oxidation of THC. However, THC marginally rises with further advancement (25.0°/30.0°). The relatively lower in-cylinder pressure and temperature results in fuel wetting at these advanced FITs due to elevated fuel penetration. Additionally, due to the SOC happening before the end of the compression stroke, there is an energy loss associated with the double compression effect, flame quenching, and excess time available for heat loss. To keep the required load condition, it is necessary to increase the amount of fuel injected. Those fuel droplets adhered to the combustion chamber walls do not take part in the main combustion event. After a delay, these adhered fuels separate from the walls, vaporize, and combust during an afterburn phase. The increase in THC emissions seen is due to the relatively less time available for the oxidation of these droplets.

Like THC, CO emissions gradually decline for the initial FIT advancement from 12.5° to 15.0°/20.0° BTDC. This is from the increasing in-cylinder temperature and ROHR for the 15.0° event compared with conventional FIT. However, CO emissions gradually increase for earlier injection events. It is well documented that CO is the primary byproduct of HC combustion, which eventually oxidizes to form CO₂ [73]. CO oxidation is preferred only after the completion of HC oxidation and the subsequent disappearance of all HC species [74]. In other words, HC oxidation inhibits the conversion of CO to CO₂. Therefore, sufficient time is necessary for CO conversion after HC oxidation. The delayed oxidation of HC in the afterburn phase deters the effective conversion of CO to CO₂. Due to this deteriorating time availability, CO emissions start to grow at 20.0° BTDC injection. Analogous to THC, there is a significant jump in CO for all EGR cases at 30.0° BTDC compared with later injections. The ID period is relatively longer for the 30.0° BTDC event. Again, the shorter time available for CO₂ formation results in elevated CO emissions.

3.4. Effect of Increasing EGR—Emissions

NO_x emissions steadily decrease with an increasing EGR rate for all FIT set points (Figure 11a). As the rate of EGR is increased, O₂ is displaced by heavier molecules, such as CO₂ and H₂O. These molecules are relatively inert and do not contribute to the exothermic combustion reaction. Additionally, they function as a heat sink and absorb the released chemical energy, hence lowering the in-cylinder temperature. The equivalence ratio gradually rises for high rates of EGR due to the displaced O₂. The combustion of relatively richer mixtures yields elevated adiabatic flame temperatures. Here, the reduction in reactivity due to the presence of CO₂ and H₂O dominates, thus resulting in lower NO_x emissions with increasing EGR. Alternatively, as discussed earlier, the lower NO_x emissions could be due to the relatively more uniform distribution of temperature in the combustion chamber. For this, the air–fuel mixture homogeneity before the SOC must gradually improve with an increasing EGR rate. The ID period at all FIT set points marginally decreases with increasing EGR, which suggests a more heterogeneous combustion process. Therefore, the PM, CO, and THC emission results obtained will provide further information to conclude that the mixture homogeneity improves with increasing EGR.

PM emissions are formed from the combustion of locally rich air–fuel mixtures (Figure 11b). Recalling the literature, using high rates of EGR typically results in elevated PM, CO, and THC emissions in the conventional combustion regime due to the

combination of a lower combustion temperature with associated combustion efficiency deterioration [43,57]. Most studies that present this a general conclusion run the engine at relatively higher loads that include both premixed and diffusion burn (i.e., mixing controlled) phases. Incomplete combustion products are relatively higher in the diffusion burn combustion phase as compared with the premixed burn phase. As explained earlier, the results presented in this study are for the purely premixed burn phase. Recalling the ID results presented in Table 3, the ID marginally decreases with the rising EGR rate used. The ID for the 0% EGR case is the highest for all the FIT set points. However, PM emissions gradually decline with increasing EGR. In general, PM emissions decrease if the formed particulates oxidize through high in-cylinder temperatures, sufficient availability of O₂, excess time available for oxidation, and relatively homogeneous and lean air–fuel mixtures surrounding the flame.

As shown in Figure 6, the peak in-cylinder temperature gradually declines with increasing EGR. In addition, elevated rates of EGR reduces the O₂ availability, as shown by the growing equivalence ratio (Figure 3). The time available for the oxidation for the particulates formed is marginally lower for high EGR rates due to the shorter ID period (Table 3). Therefore, the reducing PM emissions with rising EGR rates is due to mixture homogeneity improvements and the later combustion of the locally lean air–fuel mixture, where the maximum equivalence ratio used is 0.26. In this avenue, Lee et al. and Jadhav and Mallikarjuna suggest that the fuel evaporation rate rises with an increasing EGR rate [75,76]. They discuss that using elevated EGR rates improves the mixture fraction distribution in the combustion chamber. In addition, studies conducted by Idicheria et al. and Maiboom et al. indicate that the lift-off length increases with rising EGR rates used [77,78]. Lift-off length is the distance between the point of fuel injection and a stabilized flame location. Thus, a longer lift-off length implies that the spatial distribution of the air–fuel mixture is comparatively more uniform at high rates of EGR. Therefore, a comparatively uniform distribution of in-cylinder temperature is obtained by the instantaneous combustion of a relatively homogeneous and locally lean mixture. This results in the simultaneous reduction in NO_x and PM emissions [79,80]. This highlights the successful shift in the combustion regime from conventional to PPCI using a high-compression-ratio engine. The combination of the elevated compression ratio used in the presence of EGR aids in reducing the ID and improving the homogeneity of the air–fuel mixture simultaneously.

For all the EGR rates considered, THC and CO emissions have similar trends. Due to the differences in the trends seen with FIT variations, the THC and CO emission discussion with an increasing EGR rate is split into two parts:

- (a) Conventional FIT at 12.5° BTDC: The rising EGR rate leads to a gradual growth in THC emissions (Figure 11c). This is due to a combination of declining in-cylinder pressure, temperature, and ROHR and increasing fuel injection quantity at higher rates of EGR. Since both NO_x and PM emissions decline at higher rates of EGR, the hot EGR gases help in improving the homogeneity of the fuel. Since the SOC is close to TDC, and the combustion gases begin to rapidly expand soon after the SOC, the time available for the oxidation of THC and CO is comparatively less. In addition, the amount of O₂ available declines at high rates of EGR; hence, THC and CO emissions rise with EGR for fuel injected at 12.5° BTDC.
- (b) Earlier injection events: The THC and CO emissions for fuel injected between 12.5° and 25.0° BTDC for the 7% EGR case were marginally higher than those for the no-EGR setting. Alternatively, further increasing EGR to 14% and 25%, THC and CO emissions declined for these points. Comparable peak in-cylinder pressure, temperature, and ROHR were seen for the 7% and 14% EGR rates, as depicted in Figure 6; however, the decline in the peak performance properties was noticeable for the 25% EGR case. This suggests that the elevated in-cylinder temperature assists in forming a comparatively homogeneous mixture. In addition, the ID period for the 14% EGR case is marginally shorter than that for the 7% EGR case for this FIT. Thus, an earlier combustion onset supplies more time for THC and CO oxidation, hence lowering emissions. Moreover,

abundant O₂ is available as the air–fuel mixture is lean. As discussed earlier, fuel penetration appears to intensify for fuel injected at 25.0° and earlier for the 0% EGR case. However, there is a drop in THC for the 25.0° injection event for the 14% and 25% EGR cases. This suggests that the fuel evaporation is relatively improved, and the amount of fuel wall wetting is alleviated for the high EGR cases, hence lowering THC and CO emissions. The marginal improvement of the homogeneity of the mixture dominates and aids in lowering the THC and CO emissions. The in-cylinder pressure and temperature with respect to FIT have a bigger effect on THC and CO emissions even with high rates of EGR for fuel injected at 30.0° BTDC. It appears that CO and THC emissions were impacted the most by combustion cyclic variations as compared with PM and NO_x emissions.

Data comparing the percentage decrease in brake-specific emissions of the 25% EGR cases at earlier injection timings with that in conventional FIT without EGR are presented in Table 6. NO_x and PM for the 25% EGR case are lower than the MBT without the EGR case at nearly all FIT set points (slightly higher NO_x for the 25.0° BTDC with 25% EGR). Furthermore, CO emissions are comparable for the 20.0° and the 25.0° BTDC with the 25% EGR cases (see β in Figure 11c). In addition, THC emissions are lower for all early injection events with 25% EGR compared with that in conventional FIT with no-EGR (see α in Figure 11c). Since the NO_x and PM emissions for the 20.0° BTDC with the 25% EGR case are lower than that in conventional FIT without EGR (see λ in Figure 11a and δ in Figure 11b), the NO_x-PM trade-off is overcome. The results obtained for fuel injected between 12.5° and 20.0° BTDC with 25% EGR represent the LTC regime, and PPCI is successfully achieved.

Table 6. Percentage decrease in emissions at PPCI set points compared with conventional FIT with no-EGR for the 1.5 N-m load condition.

FIT [° BTDC] EGR [%]	NO _x [g/kW-h]	PM [g/kW-h]	CO [g/kW-h]	THC [g/kW-h]
12.5°; 25%	53.872	14.894	−40.919	−20.091
15.0°; 25%	39.407	3.036	−9.642	9.244
20.0°; 25%	7.768	40.432	0.152	20.444
25.0°; 25%	−12.592	59.193	−2.408	24.345

4. Conclusions

Due to the difficulties associated with achieving PPCI combustion through FIT adjustments alone with a high-compression-ratio engine, PPCI was tested while using EGR. Experiments were conducted to decide FIT set points and target EGR rates. Based on results obtained from an earlier study, 12.5°, 15.0°, 20.0°, 25.0°, and 30.0° BTDC were selected for the FIT sweep trial. Additionally, since the maximum achievable EGR rate at a low load condition (0.5 N-m) was 25%, intermittent rates of 7% and 14% were selected. The following are the key conclusions of the results obtained:

1. Effect of advancing FIT:
 - (a) Advancing FIT resulted in a gradual rise in the fuel amount needed to ensure a constant engine torque.
 - (b) The peak in-cylinder pressure, temperature, and ROHR gradually increased for the advancement in FIT between 12.5° and 25.0° BTDC. However, these performance parameters marginally declined for fuel injected at 30.0° BTDC due to the combustion efficiency deterioration.
 - (c) ID was slightly reduced for FIT advancement between 12.5° and 25.0° BTDC as the NTC regime of ULSD was reached. However, the ID period for the 30.0° BTDC event was respectively higher. This suggests the limit where the decreas-

ing in-cylinder temperature and pressure are too low for the instantaneous atomization and evaporation of the fuel and later ignition.

- (d) NO_x gradually increased, while PM declined with advancing FIT between 12.5° and 25.0° BTDC, hence following a traditional NO_x-PM trade-off. NO_x emissions declined, and PM grew for the 30.0° event. Overall, CO and THC emissions followed PM emission trends.
2. Effect of increasing EGR:
- (a) The equivalence ratio gradually grew with the EGR rate used for all FIT set points with the 25% EGR case about 52% to 57% higher than the no EGR case.
- (b) The peak in-cylinder pressure, temperature, and ROHR declined gradually with increasing EGR. The excess CO₂ and H₂O act as a diluent and reduce the reactivity of the charge in the cylinder, resulting in lower peak values of the performance parameters. Additionally, the amount of released energy absorbed by CO₂ and H₂O due to their higher heat capacity rises at higher rates of EGR.
- (c) The ID period marginally declined with rising EGR, suggesting that the engine's high compression ratio had a dominating effect on SOC timing. Hot EGR gases help in reducing the physical delay period.
- (d) NO_x and PM reduced simultaneously with increasing EGR at most FIT set points with 20.0° BTDC FIT and 25% EGR particularly advantageous with THC and CO also decreasing. Following the traditional definition, LTC was achieved through the PPCI method using a high-compression-ratio engine. As mentioned earlier, the ID with higher rates of EGR is marginally lower than that in the no EGR case. Hence, EGR aids in forming a relatively homogeneous air–fuel mixture. This later leads to a comparatively more uniform temperature distribution in the combustion chamber, resulting in lower NO_x emissions. Additionally, the comparatively more homogeneous mixture formed aids in lowering PM, THC, and CO emissions at high EGR rates, especially at advanced FIT set points. The relatively lean nature of the mixture and the excess time available for the oxidation of THC and CO for advanced FIT set points ensure lower incomplete combustion products even at high rates of EGR.

Finally, due to the variance inherent in real-world applications, PPCI efforts such as those presented here should be subjected to sensitivity studies based on environmental conditions to understand the entire LTC range possible.

Author Contributions: Conceptualization, C.V.S. and C.D.; methodology, C.V.S.; software, C.V.S. and S.S.A.; validation, C.V.S.; formal analysis, C.V.S.; investigation, C.V.S., S.S.A., B.S. and C.D.; resources, C.V.S. and C.D.; data curation, C.V.S.; writing—original draft preparation, C.V.S.; writing—review and editing, C.V.S., S.S.A., B.S. and C.D.; visualization, C.V.S. and C.D.; supervision, C.D.; project administration, C.D. All authors have read and agreed to the published version of the manuscript.

Funding: This research received no external funding.

Data Availability Statement: The original contributions presented in the study are included in the article, further inquiries can be directed to the corresponding author.

Conflicts of Interest: The authors declare no conflicts of interest.

Nomenclature

BSFC	brake-specific fuel consumption
BTDC	before top dead center
CI	compression ignition

CO	carbon monoxide
CO ₂	carbon dioxide
CR	compression ratio
EGR	exhaust gas recirculation
FIT	fuel injection timing
H ₂ O	water
HC	hydrocarbon
ID	ignition delay
LTC	low temperature combustion
MBT	maximum brake torque
N ₂	nitrogen
NO _x	nitrogen oxides
NTC	negative temperature coefficient
O ₂	oxygen
PM	particulate matter
PCCI	partially premixed charge compression ignition
ROHR	rate of heat release
SOC	start of combustion
THC	total hydrocarbon
ULSD	ultra-low-sulfur diesel
$\theta\text{-max}_{\text{Pressure}}$	crank angle of maximum in-cylinder pressure
$\theta\text{-max}_{\text{ROHR}}$	crank angle of maximum rate of heat release
$\theta\text{-max}_{\text{Temperature}}$	crank angle of maximum in-cylinder calculated temperature

Appendix A

Table A1. Yanmar single-cylinder engine specifications.

Manufacturer and Model	Yanmar L100V
Engine Intake	Naturally Aspirated
Fuel Intake Type	DI
Cycle	4-Stroke
Number of Cylinders	1
Number of Valves per Cylinder	1 Intake, 1 Exhaust
Bore [mm]	86
Stroke [mm]	75
Displacement [L]	0.435
CR [-]	21.2
FIT [° BTDC]	12.5 (ULSD) and 12.0 (BD)
Intermittent Rated Output at 3600 rpm [hp]	9.1
Rated Speed [rpm]	3600
Clearance Volume [m ³]	2.161×10^{-5}
Connecting Rod Length [m]	0.188
Inlet Valve Closing [° ATDC]	122
Exhaust Valve Opening [° BTDC]	144
Fuel Injection Pressure [MPa]	47 ± 2
Number of Injectors	1
Injector Holes	6

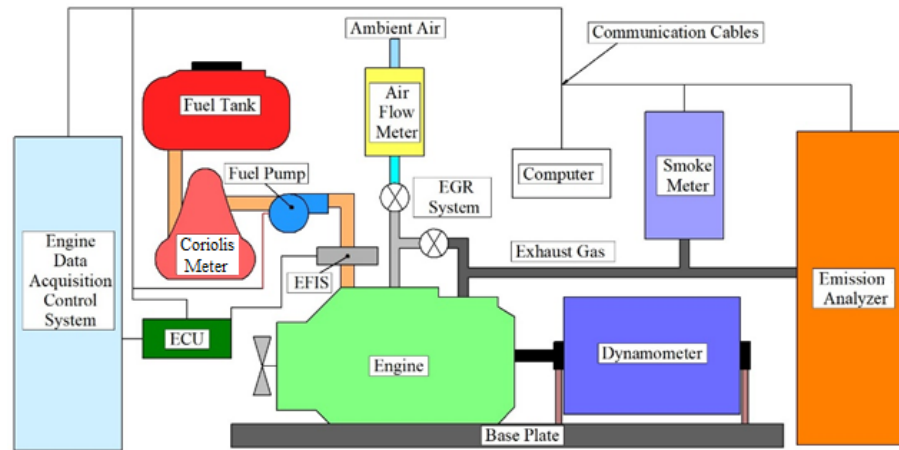


Figure A1. Block diagram of the test cell setup.

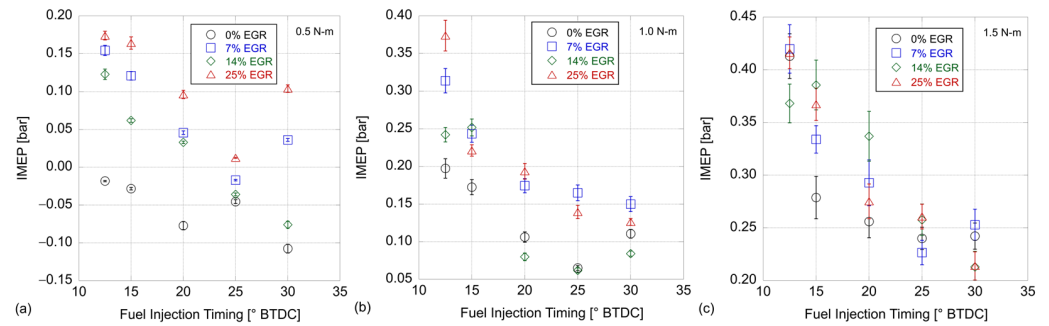


Figure A2. IMEP vs. FIT at (a) 0.5 N-m, (b) 1.0 N-m, and (c) 1.5 N-m load conditions for all EGR rates with ULSD.

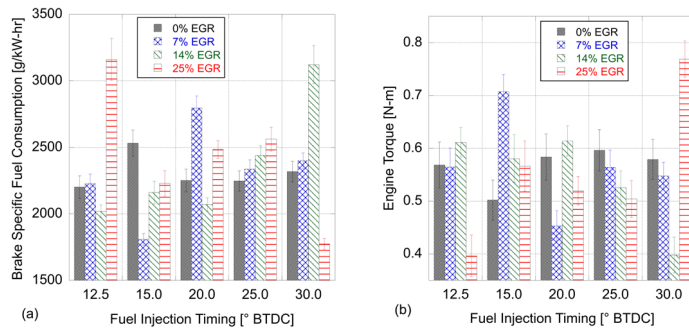


Figure A3. (a) BSFC and (b) Engine torque vs. FIT at 0.5 N-m load condition for all EGR rates with ULSD.

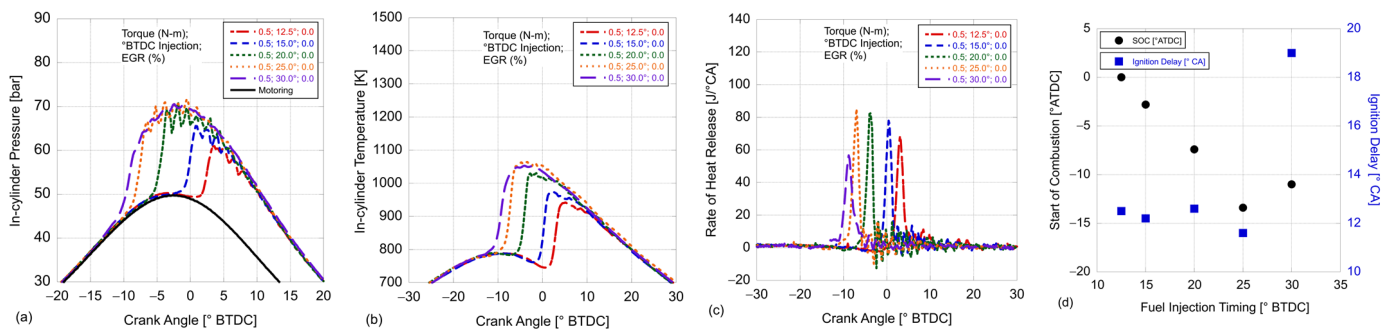


Figure A4. (a) In-cylinder pressure, (b) in-cylinder temperature, (c) ROHR, and (d) ID and SOC vs. FIT at 0.5 N-m load condition for 0% EGR with ULSD.

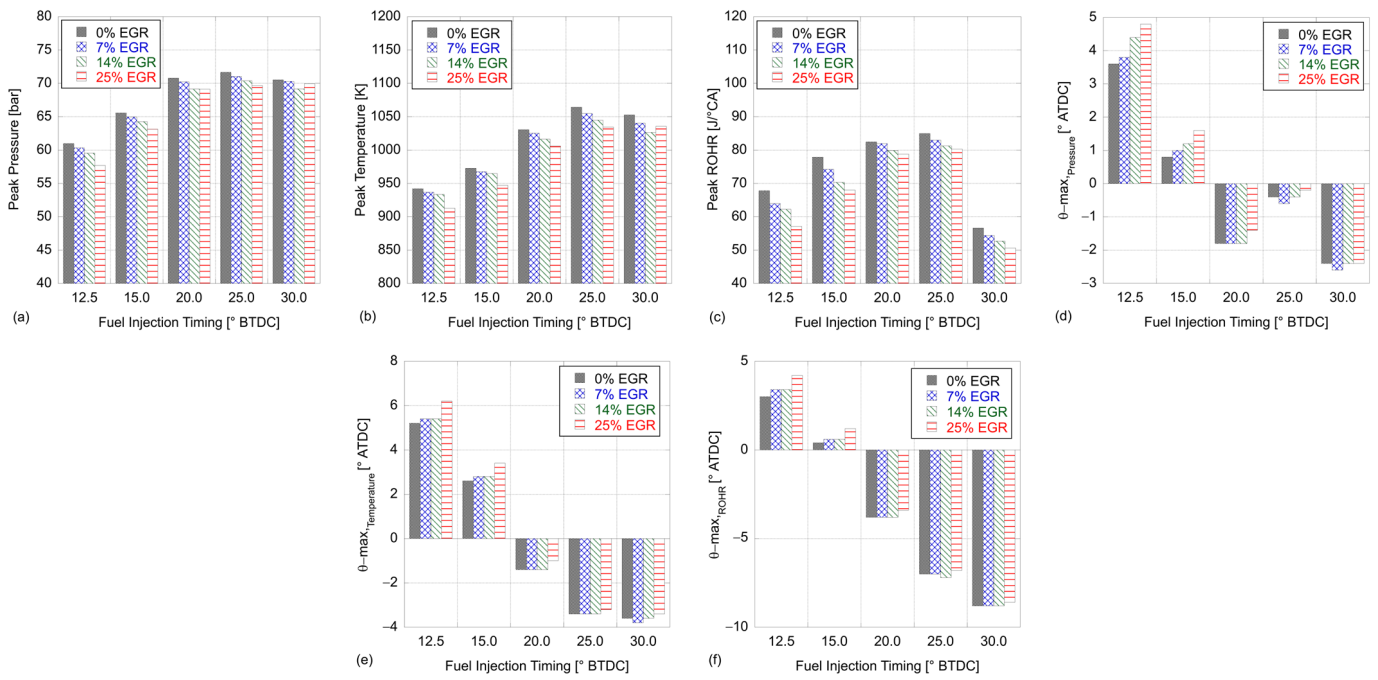


Figure A5. Peak combustion (a) pressure, (b) temperature, (c) ROHR, and corresponding crank angle position of (d) pressure, (e) temperature, and (f) ROHR vs. FIT for 0.5 N-m load condition with ULSD.

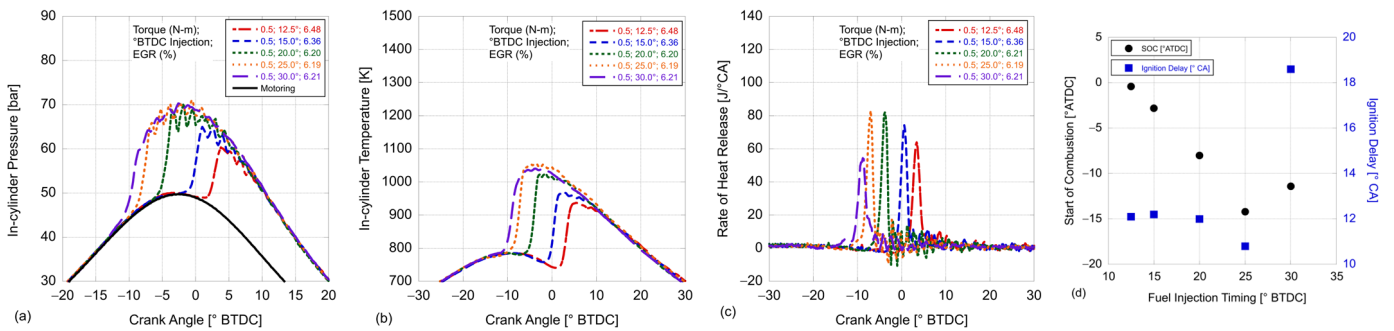


Figure A6. (a) In-cylinder pressure, (b) in-cylinder temperature, (c) ROHR, and (d) ID and SOC vs. FIT at 0.5 N-m load condition for 7% EGR with ULSD.

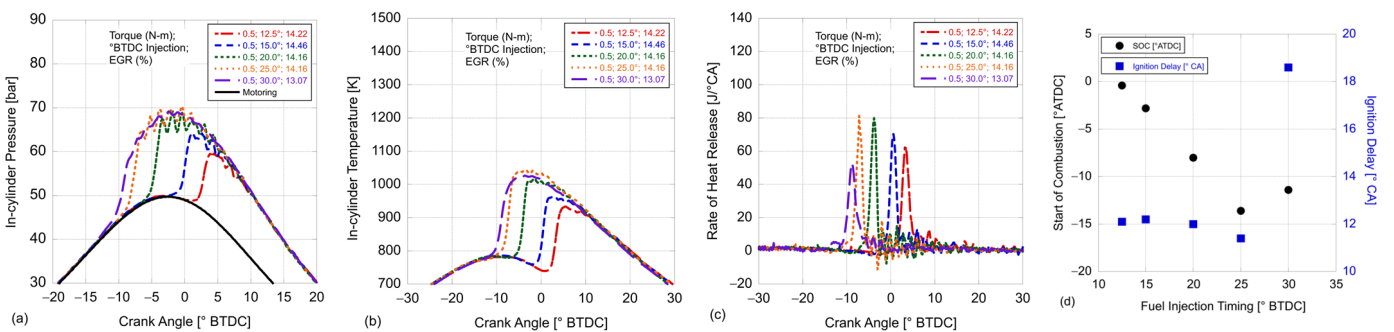


Figure A7. (a) In-cylinder pressure, (b) in-cylinder temperature, (c) ROHR, and (d) ID and SOC vs. FIT at 0.5 N-m load condition for 14% EGR with ULSD.

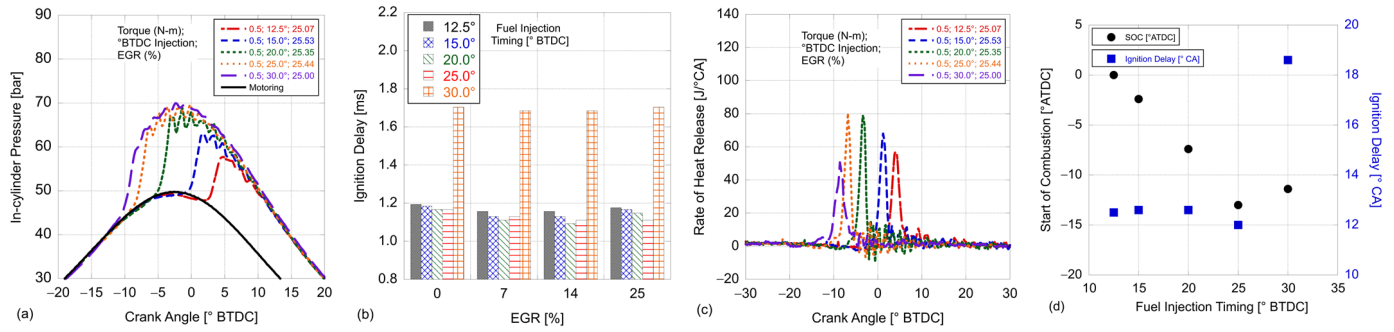


Figure A8. (a) In-cylinder pressure, (b) in-cylinder temperature, (c) ROHR, and (d) ID and SOC vs. FIT at 0.5 N-m load condition for 25% EGR with ULSD.

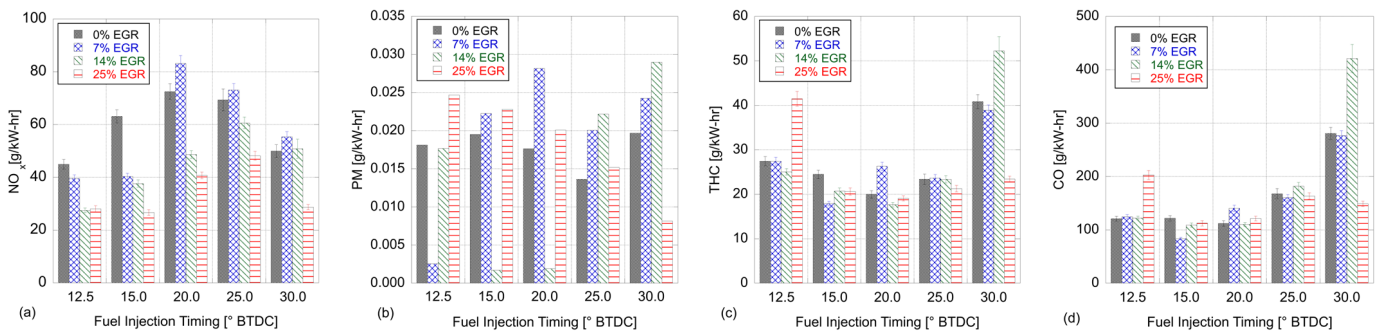


Figure A9. (a) NO_x, (b) PM, (c) CO, and (d) THC emissions for varying EGR rates at 0.5 N-m load with ULSD.

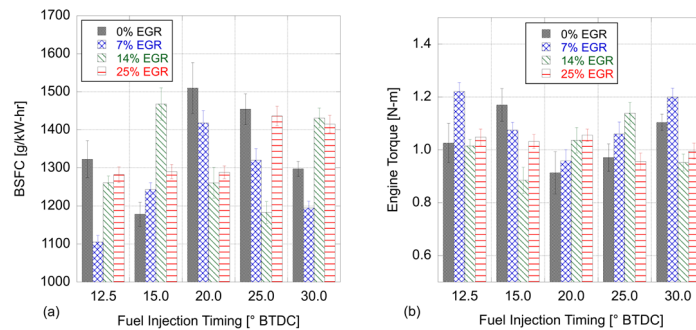


Figure A10. (a) BSFC and (b) engine torque vs. FIT at 1.0 N-m load condition for all EGR rates with ULSD.

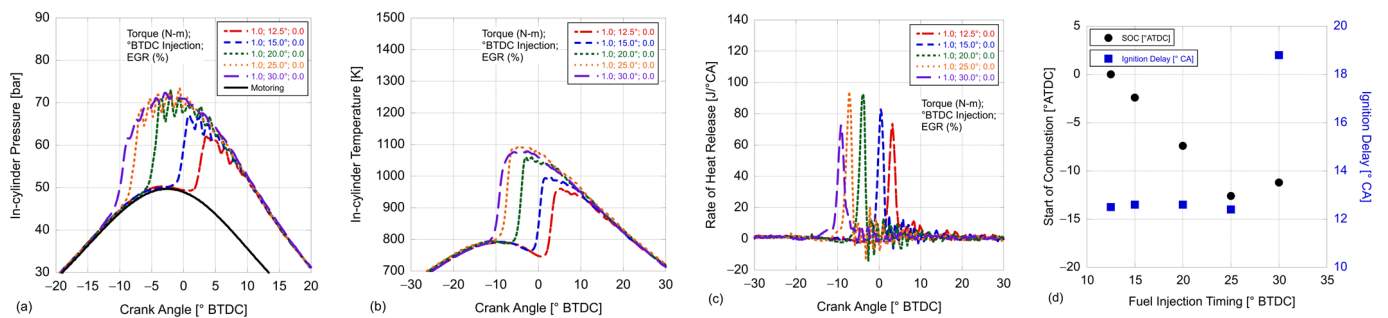


Figure A11. (a) In-cylinder pressure, (b) in-cylinder temperature, (c) ROHR, and (d) ID and SOC vs. FIT at 1.0 N-m load condition for 0% EGR with ULSD.

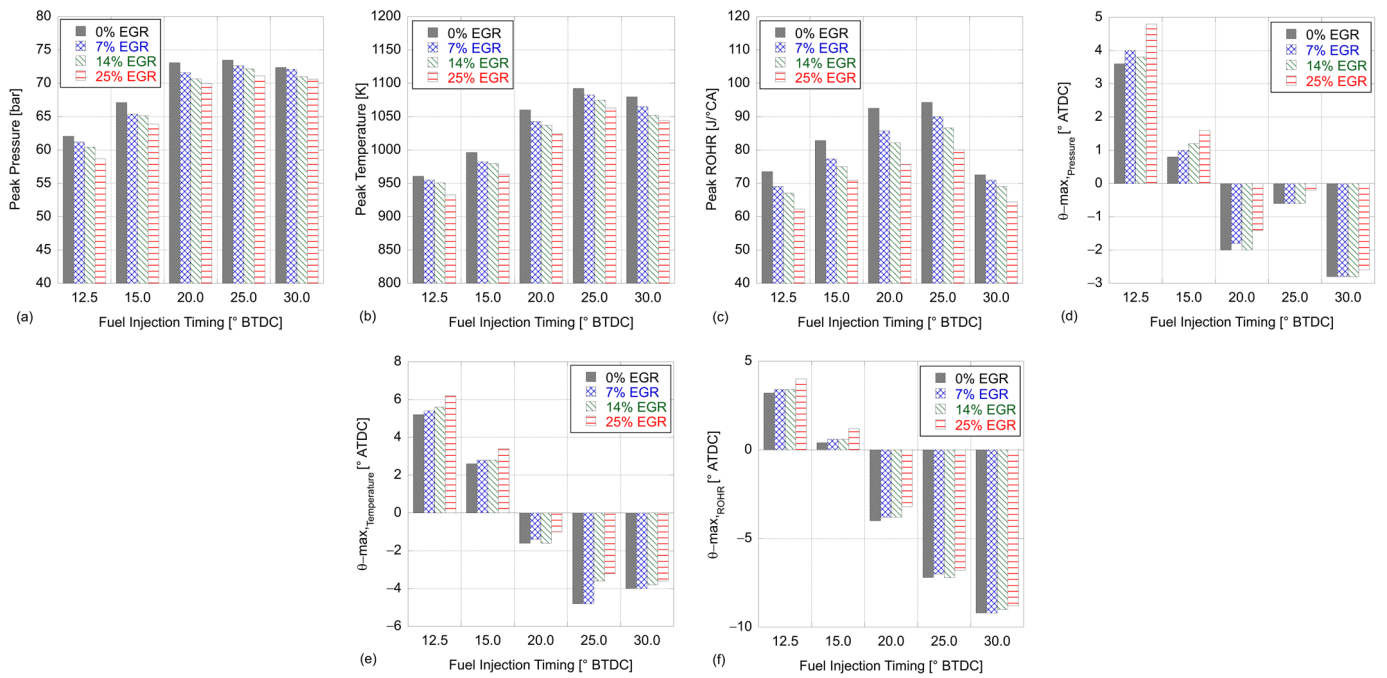


Figure A12. Peak combustion (a) pressure, (b) temperature, (c) ROHR, and corresponding crank angle position of (d) pressure, (e) temperature, and (f) ROHR vs. FIT for 1.0 N-m load condition with ULSD.

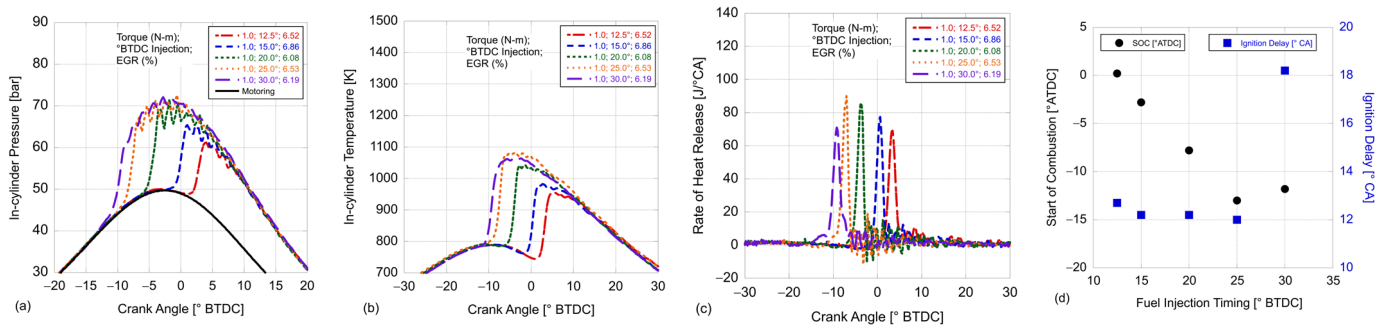


Figure A13. (a) In-cylinder pressure, (b) in-cylinder temperature, (c) ROHR, and (d) ID and SOC vs. FIT at 1.0 N-m load condition for 7% EGR with ULSD.

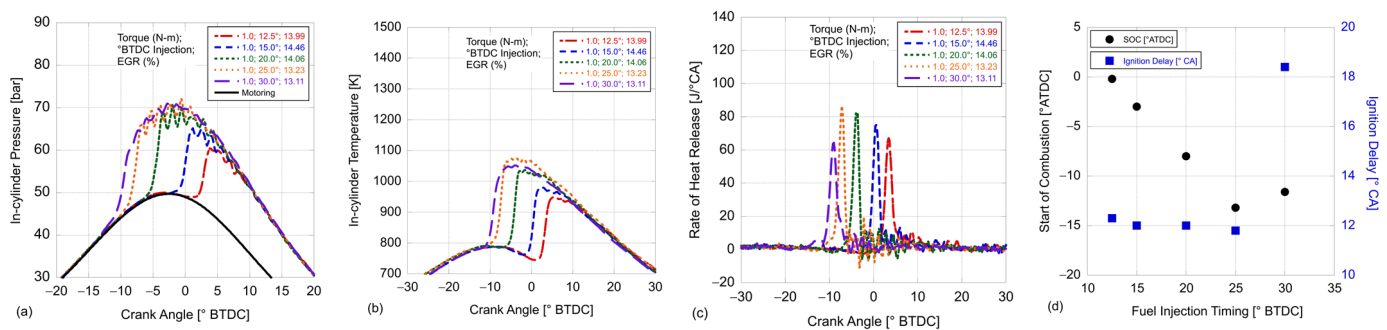


Figure A14. (a) In-cylinder pressure, (b) in-cylinder temperature, (c) ROHR, and (d) ID and SOC vs. FIT at 1.0 N-m load condition for 14% EGR with ULSD.

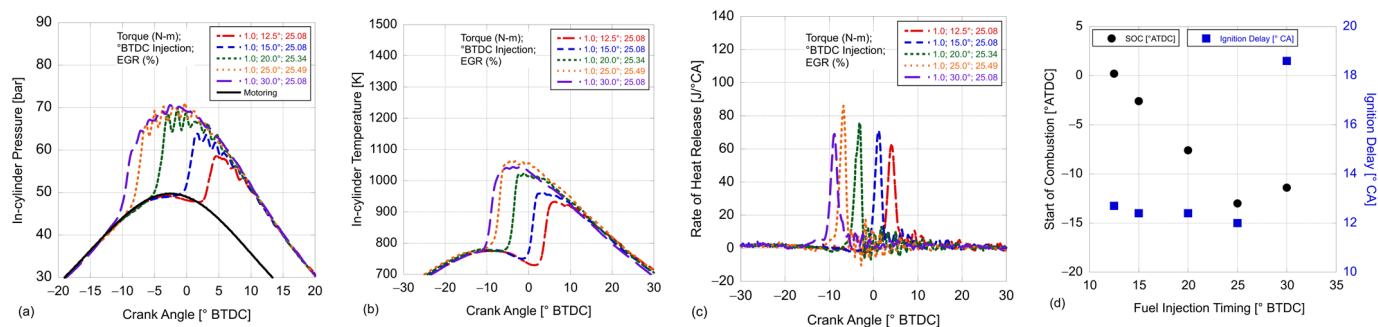


Figure A15. (a) In-cylinder pressure, (b) in-cylinder temperature, (c) ROHR, and (d) ID and SOC vs. FIT at 1.0 N-m load condition for 25% EGR with ULSD.

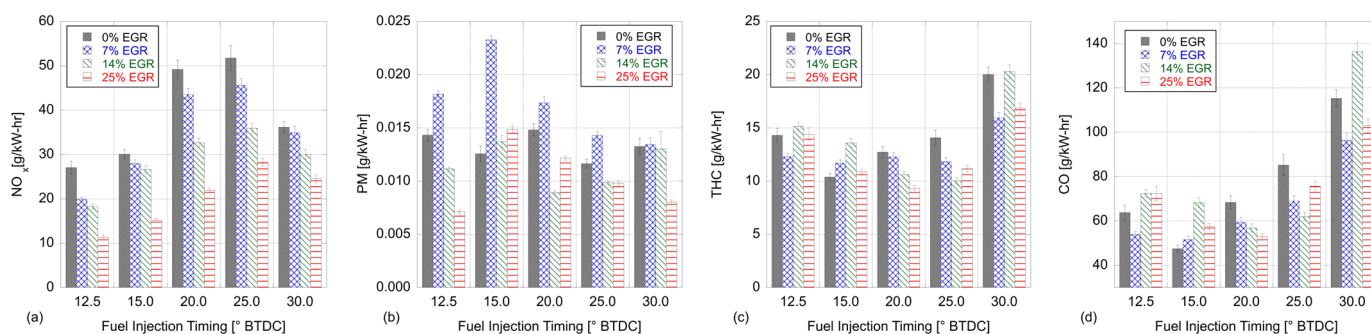


Figure A16. (a) NO_x, (b) PM, (c) CO, and (d) THC emissions for varying EGR rates at 1.0 N-m with ULSD.

References

- Hosseini, S.H.; Taghizadeh-Alisarai, A.; Ghobadian, B.; Abbaszadeh-Mayvan, A. Performance and emission characteristics of a CI engine fuelled with carbon nanotubes and diesel-biodiesel blends. *Renew. Energy* **2017**, *111*, 201–213. [\[CrossRef\]](#)
- Johnson, T.V. Diesel Emissions in Review. *SAE Int. J. Engines* **2011**, *4*, 143–157. [\[CrossRef\]](#)
- Li, Y.; Jia, M.; Chang, Y.; Fan, W.; Xie, M.; Wang, T. Evaluation of the necessity of exhaust gas recirculation employment for a methanol/diesel reactivity controlled compression ignition engine operated at medium loads. *Energy Convers. Manag.* **2015**, *101*, 40–51. [\[CrossRef\]](#)
- Elsanusi, O.A.; Roy, M.M.; Sidhu, M.S. Experimental Investigation on a Diesel Engine Fueled by Diesel-Biodiesel Blends and their Emulsions at Various Engine Operating Conditions. *Appl. Energy* **2017**, *203*, 582–593. [\[CrossRef\]](#)
- Kiplimo, R.; Tomita, E.; Kawahara, N.; Yokobe, S. Effects of spray impingement, injection parameters, and EGR on the combustion and emission characteristics of a PCCI diesel engine. *Appl. Therm. Eng.* **2012**, *37*, 165–175. [\[CrossRef\]](#)
- Genzale, C.L.; Reitz, R.D.; Musculus, M.P. Effects of spray targeting on mixture development and emissions formation in late-injection low-temperature heavy-duty diesel combustion. *Proc. Combust. Inst.* **2009**, *32*, 2767–2774. [\[CrossRef\]](#)
- Genzale, C.; Reitz, R.; Musculus, M. Effects of Piston Bowl Geometry on Mixture Development and Late-Injection Low-Temperature Combustion in a Heavy-Duty Diesel Engine. *SAE Int. J. Engines* **2009**, *1*, 913–937. [\[CrossRef\]](#)
- Dimitriou, P.; Wang, W.; Peng, Z. A Piston Geometry and Nozzle Spray Angle Investigation in a DI Diesel Engine by Quantifying the Air-Fuel Mixture. *Int. J. Spray Combust. Dyn.* **2015**, *7*, 1–24. [\[CrossRef\]](#)
- Hsu, B. *Practical Diesel-Engine Combustion Analysis*; SAE International: Warrendale, PA, USA, 2002.
- Heywood, J.B. *Internal Combustion Engine Fundamentals*, 2nd ed.; McGraw-Hill Education: New York, NY, USA, 2018.
- Cheikh, K.; Sary, A.; Khaled, L.; Abdelkrim, L.; Mohand, T. Experimental assessment of performance and emissions maps for biodiesel fueled compression ignition engine. *Appl. Energy* **2016**, *161*, 320–329. [\[CrossRef\]](#)
- Tan, P.-Q.; Ruan, S.-S.; Hu, Z.-Y.; Lou, D.-M.; Li, H. Particle number emissions from a light-duty diesel engine with biodiesel fuels under transient-state operating conditions. *Appl. Energy* **2014**, *113*, 22–31. [\[CrossRef\]](#)
- Dec, J.E. *A Conceptual Model of DI Diesel Combustion Based on Laser-Sheet Imaging*; SAE Paper 970873; SAE International: Warrendale, PA, USA, 1997. [\[CrossRef\]](#)
- Dec, J.E.; Espey, C. *Chemiluminescence Imaging of Autoignition in a DI Diesel Engine*; SAE International: Warrendale, PA, USA, 1998. [\[CrossRef\]](#)
- Yang, K.; Nishida, K.; Yamakawa, H. Effect of split injection ratio on combustion process of diesel spray into two-dimensional piston cavity. *Fuel* **2020**, *260*, 116316. [\[CrossRef\]](#)

16. Ramalingam, S.; Babu, D.; Santhoshkumar, A.; Deepakkumar, R.; Ravikanth, D. Impact of exhaust gas recirculation and split injection strategy combustion behavior on premixed charge compression ignition engine fuelled with moringa oleifera methyl ester. *Fuel* **2022**, *319*, 123702. [[CrossRef](#)]
17. Srivatsa, C.V.; Mattson, J.; Depcik, C. Exploring the Possibility of Achieving Partially Premixed Charge Compression Ignition Combustion of Biodiesel in Comparison to Ultra Low Sulfur Diesel on a High Compression Ratio Engine. *Combust. Sci. Technol.* **2023**, *195*, 746–777. [[CrossRef](#)]
18. Pachiannan, T.; Zhong, W.; Rajkumar, S.; He, Z.; Leng, X.; Wang, Q. A literature review of fuel effects on performance and emission characteristics of low-temperature combustion strategies. *Appl. Energy* **2019**, *251*, 113380. [[CrossRef](#)]
19. Splitter, D.; Kokjohn, S.; Rein, K.; Hanson, R.; Sanders, S.; Reitz, R.D. An Optical Investigation of Ignition Processes in Fuel Reactivity Controlled PCCI Combustion. *SAE Int. J. Engines* **2010**, *3*, 142–162. [[CrossRef](#)]
20. Shim, E.; Park, H.; Bae, C. Comparisons of advanced combustion technologies (HCCI, PCCI, and dual-fuel PCCI) on engine performance and emission characteristics in a heavy-duty diesel engine. *Fuel* **2020**, *262*, 116436. [[CrossRef](#)]
21. Silke, E.J.; Pitz, W.J.; Westbrook, C.K.; Sjöberg, M.; Dec, J.E. Understanding the Chemical Effects of Increased Boost Pressure under HCCI Conditions. *SAE Int. J. Fuels Lubr.* **2008**, *1*, 12–25. [[CrossRef](#)]
22. Wang, Y.; Wang, H.; Yao, M. Effects of low-temperature reforming products of PRF50 on combustion and emission characteristics in an HCCI engine. *Appl. Therm. Eng.* **2019**, *151*, 451–458. [[CrossRef](#)]
23. Veza, I.; Irianto; Tuan Hoang, A.; Yusuf, A.A.; Herawan, S.G.; Soudagar, M.E.M.; Samuel, O.D.; Said, M.F.M.; Silitonga, A.S. Effects of Acetone-Butanol-Ethanol (ABE) addition on HCCI-DI engine performance, combustion and emission. *Fuel* **2023**, *333*, 126377. [[CrossRef](#)]
24. Kokjohn, S.L.; Musculus, M.P.B.; Reitz, R.D. Evaluating temperature and fuel stratification for heat-release rate control in a reactivity-controlled compression-ignition engine using optical diagnostics and chemical kinetics modeling. *Combust. Flame* **2015**, *162*, 2729–2742. [[CrossRef](#)]
25. Pandian, M.M.; Anand, K. Experimental optimization of reactivity controlled compression ignition combustion in a light duty diesel engine. *Appl. Therm. Eng.* **2018**, *138*, 48–61. [[CrossRef](#)]
26. Benajes, J.; Molina, S.; García, A.; Belarte, E.; Vanvolsem, M. An investigation on RCCI combustion in a heavy duty diesel engine using in-cylinder blending of diesel and gasoline fuels. *Appl. Therm. Eng.* **2014**, *63*, 66–76. [[CrossRef](#)]
27. Padala, S.; Woo, C.; Kook, S.; Hawkes, E.R. Ethanol utilisation in a diesel engine using dual-fuelling technology. *Fuel* **2013**, *109*, 597–607. [[CrossRef](#)]
28. Liu, J.; Ma, H.; Wang, L.; Liang, W.; Ji, Q.; Sun, P.; Wang, P. Effects of EGR on combustion and emission characteristics of PODE/methanol RCCI mode at high load. *Appl. Therm. Eng.* **2023**, *223*, 120036. [[CrossRef](#)]
29. Jena, A.; Sonawane, U.; Agarwal, A.K. Partially premixed combustion of diesel-di-ethyl ether blends in light-duty commercial engine. *Fuel* **2023**, *345*, 128197. [[CrossRef](#)]
30. Kalghatgi, G.T.; Hildingsson, L.; Harrison, A.J.; Johansson, B. Autoignition quality of gasoline fuels in partially premixed combustion in diesel engines. *Proc. Combust. Inst.* **2011**, *33*, 3015–3021. [[CrossRef](#)]
31. Kalghatgi, G.T. The outlook for fuels for internal combustion engines. *Int. J. Engine Res.* **2014**, *15*, 383–398. [[CrossRef](#)]
32. Kalghatgi, G.; Agarwal, A.K.; Goyal, H.; Houidi, M.B. *Introduction to Gasoline Compression Ignition Technology: Future Prospects*; Springer Nature: Singapore, 2022.
33. Park, H.; Shim, E.; Bae, C. Improvement of combustion and emissions with exhaust gas recirculation in a natural gas-diesel dual-fuel premixed charge compression ignition engine at low load operations. *Fuel* **2019**, *235*, 763–774. [[CrossRef](#)]
34. Pratap Singh, A.; Jena, A.; Agarwal, A.K. Multiple fuel injection strategy for premixed charge compression ignition combustion engine using biodiesel blends. *Int. J. Engine Res.* **2022**, *24*, 888–903. [[CrossRef](#)]
35. Singh, A.P.; Agarwal, A.K. Performance and emission characteristics of conventional diesel combustion/partially premixed charge compression ignition combustion mode switching of biodiesel-fueled engine. *Int. J. Engine Res.* **2019**, *22*, 540–553. [[CrossRef](#)]
36. Qiu, L.; Cheng, X.; Liu, B.; Dong, S.; Bao, Z. Partially premixed combustion based on different injection strategies in a light-duty diesel engine. *Energy* **2016**, *96*, 155–165. [[CrossRef](#)]
37. An, Y.; Jaasim, M.; Raman, V.; Hernández Pérez, F.E.; Sim, J.; Chang, J.; Im, H.G.; Johansson, B. Homogeneous charge compression ignition (HCCI) and partially premixed combustion (PPC) in compression ignition engine with low octane gasoline. *Energy* **2018**, *158*, 181–191. [[CrossRef](#)]
38. Goyal, H.; Panthi, N.; Almanashi, A.; Magnotti, G. Influence of fuel injection parameters at low-load conditions in a partially premixed combustion (PPC) based heavy-duty optical engine. *Appl. Therm. Eng.* **2023**, *232*, 121049. [[CrossRef](#)]
39. Bobi, S.; Kashif, M.; Laonual, Y. Combustion and emission control strategies for partially-premixed charge compression ignition engines: A review. *Fuel* **2022**, *310*, 122272. [[CrossRef](#)]
40. Srivatsa, C.V.; Mattson, J.; Depcik, C. Performance and Emission Analysis of Partially Premixed Charge Compression Ignition Combustion. *J. Eng. Gas Turbines Power* **2019**, *141*, 061004. [[CrossRef](#)]
41. Thangaraja, J.; Kannan, C. Effect of exhaust gas recirculation on advanced diesel combustion and alternate fuels—A review. *Appl. Energy* **2016**, *180*, 169–184. [[CrossRef](#)]

42. Kim, J.; Jang, J.; Lee, K.; Lee, Y.; Oh, S.; Lee, S. Combustion and emissions characteristics of Diesel and soybean biodiesel over wide ranges of intake pressure and oxygen concentration in a compression–ignition engine at a light-load condition. *Fuel* **2014**, *129*, 11–19. [[CrossRef](#)]
43. Zhu, H.; Bohac, S.V.; Huang, Z.; Assanis, D.N. Defeat of the soot/NO_x trade-off using biodiesel-ethanol in a moderate exhaust gas recirculation premixed low-temperature combustion mode. *J. Eng. Gas Turbines Power* **2013**, *135*, 091502. [[CrossRef](#)]
44. Veltman, M.K.; Karra, P.K.; Kong, S.-C. *Effects of Biodiesel Blends on Emissions in Low Temperature Diesel Combustion*; 0148-7191; SAE Technical Paper: 38; SAE International: Warrendale, PA, USA, 2009. [[CrossRef](#)]
45. Hunicz, J.; Matijošius, J.; Rimkus, A.; Kilikevičius, A.; Kordos, P.; Mikulski, M. Efficient hydrotreated vegetable oil combustion under partially premixed conditions with heavy exhaust gas recirculation. *Fuel* **2020**, *268*, 117350. [[CrossRef](#)]
46. Jiménez-Espadafor, F.J.; Torres, M.; Velez, J.A.; Carvajal, E.; Becerra, J.A. Experimental analysis of low temperature combustion mode with diesel and biodiesel fuels: A method for reducing NO_x and soot emissions. *Fuel Process. Technol.* **2012**, *103*, 57–63. [[CrossRef](#)]
47. Tompkins, B.T.; Jacobs, T.J. Low-temperature combustion with biodiesel: Its enabling features in improving efficiency and emissions. *Energy Fuels* **2013**, *27*, 2794–2803. [[CrossRef](#)]
48. Tompkins, B.T.; Song, H.; Jacobs, T.J. Low temperature heat release of palm and soy biodiesel in late injection low temperature combustion. *SAE Int. J. Fuels Lubr.* **2014**, *7*, 106–115. [[CrossRef](#)]
49. Su, J.; Zhu, H.; Bohac, S.V. Particulate matter emission comparison from conventional and premixed low temperature combustion with diesel, biodiesel and biodiesel–ethanol fuels. *Fuel* **2013**, *113*, 221–227. [[CrossRef](#)]
50. Cao, D.N.; Hoang, A.T.; Luu, H.Q.; Bui, V.G.; Tran, T.T.H. Effects of injection pressure on the NO_x and PM emission control of diesel engine: A review under the aspect of PCCI combustion condition. In *Energy Sources, Part A: Recovery, Utilization, and Environmental Effects*; Taylor & Francis: Oxfordshire, UK, 2020; pp. 1–18. [[CrossRef](#)]
51. Zheng, M.; Mulenga, M.C.; Reader, G.T.; Wang, M.; Ting, D.S.K.; Tjong, J. Biodiesel engine performance and emissions in low temperature combustion. *Fuel* **2008**, *87*, 714–722. [[CrossRef](#)]
52. Zheng, M.; Han, X.; Tan, Y.; Kobler, M.S.; Ko, S.-J.; Wang, M.; Mulenga, M.C.; Tjong, J. *Low Temperature Combustion of Neat Biodiesel Fuel on a Common-Rail Diesel Engine*; 0148-7191; SAE Technical Paper: 33; SAE International: Warrendale, PA, USA, 2008. [[CrossRef](#)]
53. Rohani, B.; Park, S.S.; Bae, C. Effect of injection strategy on smoothness, emissions and soot characteristics of PCCI-conventional diesel mode transition. *Appl. Therm. Eng.* **2016**, *93*, 1033–1042. [[CrossRef](#)]
54. Lee, S.; Jang, J.; Oh, S.; Lee, Y.; Kim, J.; Lee, K. *Comparative Study on Effect of Intake Pressure on Diesel and Biodiesel Low Temperature Combustion Characteristics in a Compression Ignition Engine*; 0148-7191; SAE Technical Paper: 45; SAE International: Warrendale, PA, USA, 2013. [[CrossRef](#)]
55. Jain, A.; Singh, A.P.; Agarwal, A.K. Effect of fuel injection parameters on combustion stability and emissions of a mineral diesel fueled partially premixed charge compression ignition (PCCI) engine. *Appl. Energy* **2017**, *190*, 658–669. [[CrossRef](#)]
56. Karra, P.K.; Veltman, M.K.; Kong, S.-C. Characteristics of engine emissions using biodiesel blends in low-temperature combustion regimes. *Energy Fuels* **2008**, *22*, 3763–3770. [[CrossRef](#)]
57. Weall, A.; Collings, N. Highly homogeneous compression ignition in a direct injection diesel engine fuelled with diesel and biodiesel. In *SAE Transactions*; SAE International: Warrendale, PA, USA, 2007; pp. 646–660. [[CrossRef](#)]
58. Zheng, M.; Mulenga, M.C.; Reader, G.T.; Wang, M.; Ting, D.S. *Influence of Biodiesel Fuel on Diesel Engine Performance and Emissions in Low Temperature Combustion*; 0148-7191; SAE Technical Paper: 48; SAE International: Warrendale, PA, USA, 2006. [[CrossRef](#)]
59. Azad, A.K.; Doppalapudi, A.T.; Khan, M.M.K.; Hassan, N.M.S.; Gudimetla, P. A landscape review on biodiesel combustion strategies to reduce emission. *Energy Rep.* **2023**, *9*, 4413–4436. [[CrossRef](#)]
60. Cheung, C.; Zhu, L.; Huang, Z. Regulated and unregulated emissions from a diesel engine fueled with biodiesel and biodiesel blended with methanol. *Atmos. Environ.* **2009**, *43*, 4865–4872. [[CrossRef](#)]
61. Appavu, P.; Ramanan, M.V.; Jayaraman, J.; Venu, H. NO_x emission reduction techniques in biodiesel-fuelled CI engine: A review. *Aust. J. Mech. Eng.* **2021**, *19*, 210–220. [[CrossRef](#)]
62. Tazua, X.; Maiboom, A.; Shah, S.R. Experimental study of inlet manifold water injection on combustion and emissions of an automotive direct injection diesel engine. *Energy* **2010**, *35*, 3628–3639. [[CrossRef](#)]
63. Langness, C.; Srivatsa, C.; Depcik, C. *Design and Control of an Automated Cooled Exhaust Gas Recirculation System for a Teaching and Research Engine Test Cell*; SAE International: Warrendale, PA, USA, 2018.
64. Mangus, M.D. *Implementation of Engine Control and Measurement Strategies for Biofuel Research in Compression-Ignition Engines*; University of Kansas: Lawrence, KS, USA, 2014.
65. Ceclre, E.D. *Controls and Measurements of KU Engine Test Cells for Biodiesel, SynGas, and Assisted Biodiesel Combustion*; University of Kansas: Lawrence, KS, USA, 2011.
66. Srivatsa, C.V. *Comparison of Ultra-Low Sulfur Diesel and Biodiesel Combustion Characteristics in the Partially Premixed Charge Compression Ignition Regime*; University of Kansas: Lawrence, KS, USA, 2022.
67. Mattson, J.M.S. *Power, Efficiency, and Emissions Optimization of a Single Cylinder Direct-Injected Diesel Engine for Testing of Alternative Fuels through Heat Release Modeling*; University of Kansas: Lawrence, KS, USA, 2013.
68. Fang, T.; Lin, Y.C.; Foong, T.M.; Lee, C.F. Reducing NO_x Emissions from a Biodiesel-Fueled Engine by Use of Low-Temperature Combustion. *Environ. Sci. Technol.* **2008**, *42*, 8865–8870. [[CrossRef](#)] [[PubMed](#)]

69. Gowdagiri, S.; Wang, W.; Oehlschlaeger, M.A. A shock tube ignition delay study of conventional diesel fuel and hydroprocessed renewable diesel fuel from algal oil. *Fuel* **2014**, *128*, 21–29. [[CrossRef](#)]
70. Luong, M.B.; Pérez, F.E.H.; Im, H.G. Prediction of ignition modes of NTC-fuel/air mixtures with temperature and concentration fluctuations. *Combust. Flame* **2020**, *213*, 382–393. [[CrossRef](#)]
71. Naidja, A.; Krishna, C.; Butcher, T.; Mahajan, D. Cool flame partial oxidation and its role in combustion and reforming of fuels for fuel cell systems. *Prog. Energy Combust. Sci.* **2003**, *29*, 155–191. [[CrossRef](#)]
72. Ranzi, E.; Dente, M.; Goldaniga, A.; Bozzano, G.; Faravelli, T. Lumping procedures in detailed kinetic modeling of gasification, pyrolysis, partial oxidation and combustion of hydrocarbon mixtures. *Prog. Energy Combust. Sci.* **2001**, *27*, 99–139. [[CrossRef](#)]
73. Westbrook, C.K.; Dryer, F.L. Chemical kinetic modeling of hydrocarbon combustion. *Prog. Energy Combust. Sci.* **1984**, *10*, 1–57. [[CrossRef](#)]
74. Glassman, I.; Yetter, R.A.; Glumac, N.G. *Combustion*; Academic Press: Cambridge, MA, USA, 2014.
75. Lee, Y.; Huh, K.Y. Analysis of different modes of low temperature combustion by ultra-high EGR and modulated kinetics in a heavy duty diesel engine. *Appl. Therm. Eng.* **2014**, *70*, 776–787. [[CrossRef](#)]
76. Jadhav, P.D.; Mallikarjuna, J. *Effect of EGR on Performance and Emission Characteristics of a GDI Engine-A CFD Study*; 0148-7191; SAE Technical Paper; SAE International: Warrendale, PA, USA, 2017. [[CrossRef](#)]
77. Idicheria, C.A.; Pickett, L.M. Effect of EGR on diesel premixed-burn equivalence ratio. *Proc. Combust. Inst.* **2007**, *31*, 2931–2938. [[CrossRef](#)]
78. Maiboom, A.; Tauzia, X.; Hétet, J.-F.; Cormerais, M.; Tounsi, M.; Jaine, T.; Blanchin, S. *Various Effects of EGR on Combustion and Emissions on an Automotive DI Diesel Engine: Numerical and Experimental Study*; 0148-7191; SAE Technical Paper; SAE International: Warrendale, PA, USA, 2007. [[CrossRef](#)]
79. Dickey, D.W.; Ryan, T.W., III; Matheaus, A.C. *NOx Control in Heavy-Duty Diesel Engines—What Is the Limit?* SAE Paper 980174; SAE International: Warrendale, PA, USA, 1998. [[CrossRef](#)]
80. Ryan, T.W., III; Callahan, T.J. *Homogeneous Charge Compression Ignition of Diesel Fuel*; SAE Paper 961160; SAE International: Warrendale, PA, USA, 1996. [[CrossRef](#)]

Disclaimer/Publisher’s Note: The statements, opinions and data contained in all publications are solely those of the individual author(s) and contributor(s) and not of MDPI and/or the editor(s). MDPI and/or the editor(s) disclaim responsibility for any injury to people or property resulting from any ideas, methods, instructions or products referred to in the content.